RECOVERY OF METAL AND ENERGY FROM CAPACITIVE DEIONIZATION (CDI) DISCHARGED BRINE

by

Md. Sazal Miah

A Thesis Submitted in Partial Fulfillment of the Requirements for the

Degree of Master of Engineering in Nanotechnology

Examination Committee:	Dr. Tanujjal Bora (Chairperson) Dr. Chanchana Thanachayanont Dr. Raffaele Ricco
Nationality:	Bangladeshi
Previous Degree:	Bachelor of Science in Electrical and Electronics Engineering The University of Asia Pacific Dhaka, Bangladesh
Scholarship Donor:	His Majesty the King's Scholarship (Thailand)

Asian Institute of Technology
School of Engineering and Technology
Thailand
July 2022

AUTHOR'S DECLARATION

I, Md. Sazal Miah, declare that the research work carried out for this thesis was in accordance with the regulations of the Asian Institute of Technology. The work presented in it are my own and has been generated by me as the result of my own original research, and if external sources were used, such sources have been cited. It is original and has not been submitted to any other institution to obtain another degree or qualification. This is a true copy of the thesis, including final revisions.

Date: July 14, 2022

Name (in printed letters): Md. Sazal Miah

Signature: 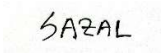

ACKNOWLEDGMENTS

First and foremost, I am very much grateful to the almighty Allah for his blessings on me for completing my thesis and master's degree.

I would like to offer my heartfelt gratitude to my advisor, Dr. Tanujjal Bora, for his continuous guidance, valuable suggestions, dedication, and encouragement during my research that motivated me to complete this work. It is not only his advice to me regarding the scientific aspects but also the constructive criticism he offered in various stages of the research that helped me keep myself on the right track towards fulfilling the goals.

I am thankful to Dr. Raffaele Ricco for his informative and inspirational suggestions and kind support. I would like to extend my sincere thanks to the Nanogroup members, Mr. Santi, Mr. Wisanu, Mr. Napatsakorn, Ms. Sirada, Mr. Peerawich, Mr. Anan, Ms. Apichaya, Mr. Kaiyum, and Mr. Manish, for their help, support, blessing and for maintaining such a friendly environment in the laboratory.

It is honorable for me to thank Royal Thai Government for the financial support that provided me an opportunity to study at the Asian Institute of Technology (AIT).

Last but not least, I am immensely grateful to my warm family, my parents, and my brother for their love, continuous support, wishes, and sacrifices throughout this journey. I want to thank my beloved wife, Tania, for her constant support and inspiration to continue my study at AIT.

ABSTRACT

Activated carbon cloth (ACC) electrodes modified with manganese dioxide (MnO_2) are used in capacitive deionization (CDI), a promising strategy for conducting metal and energy recovery along with desalination. The removal capability of copper (Cu^{2+}), Nickel (Ni^{2+}), and Chromium (Cr^{2+}) ions and their recovery in the metallic form are examined. Multiple important concerns have been investigated to test the feasibility of CDI metal recovery from a practical point of view, like the impact of the voltage on the ion adsorption, metal recovery, the concentration of metal ions, and its long-term viability. During the charging step of the CDI cell, some energy is stored in the carbon electrode, and this energy can be further recovered during the discharging phase. In this thesis, an energy recovery mechanism is developed and investigated to recover the energy during the desorption step by utilizing a four-switch buck-boost converter as a DC/DC converter and a supercapacitor (SC) as the energy storage device. A basic CDI cell is constructed to perform the above experiments. Faraday's laws of electrolysis and atomic absorption spectroscopy (AAS) analysis are performed to understand the Cu^{2+} and Cr^{3+} deposition efficiency during metal recovery in the form of electroplating, and to find out the appropriate voltage and pH range. Lastly, energy recovery efficiency analysis is performed to assess the amount of energy that can actually be recovered from the CDI cell.

Keywords: capacitive deionization, metal recovery, energy recovery, desalination

CONTENTS

LIST OF TABLES

LIST OF FIGURES

Page

LIST OF ABBREVIATIONS

AAS = Atomic Absorption Spectroscopy

ACC = Activated Carbon Cloth

CDI = Capacitive Deionization

CV = Charging Voltage

EDL = Electric Double Layer

FCDI = Flow-Electrode CDI

MCDI = Membrane CDI

NOM = Natural Organic Matter

SC = Supercapacitor

SSA = Specific Surface Area

CHAPTER 1
INTRODUCTION

1.1 Background of the Study

The rising need for energy and water has been a serious global problem due to fast population growth and ever-changing technological progress. Based on the United Nations' Sustainable Development Goals (SDGs) (Griggs et al., 2013), water and energy have been identified as two critical problems. Hence, in recent years, the interdependence of energy and water has been a vital concern (DeNooyer et al., 2016; Fang & Chen, 2017; Shang et al., 2018). Human beings are also at risk of exposure to heavy metals from various sources in their daily activities (Vardhan et al., 2019).

Even though few of them are beneficial, they can cause acute and chronic health effects that can be either fatal or long-lasting. Copper ion (Cu^{2+}), chromium ion (Cr^{2+}), and nickel (Ni^{2+}) are hazardous contaminants that are produced in a variety of industries, including printing circuits, plating, metallurgy, and mining (Zhan et al., 2011). Cu^{2+} discharge into inland surface waters has a tolerance limit of 3.0 mg/L, while the drinking water has a tolerance limit of 0.05 mg/L (Huang & Su, 2010). As a result, removing Cu^{2+} from water was critical, and many technologies have been developed (Z. Chen et al., 2015; Dehkhoda et al., 2016). Although, several efforts have been put into developing methods for purifying Cu^{2+} containing effluents, minimal emphasis has been paid to the recovery of metallic copper from the contaminated water for sale and reuse.

Heavy metal and energy recovery from polluted water or wastewater can be accomplished using a variety of methods. Each has its own set of benefits and compatibility with various water treatment methods. However, most of these technologies still have flaws that limit their effectiveness as a heavy metal pollution countermeasure under the influence of the water crisis. In terms of the traditional capacitive deionization (CDI) system, one pair of activated carbon (AC) porous electrodes are widely used. And ionic components are mostly confined inside the electric double layer (EDL) of the electrode’s inner pores when an electric field was supplied externally (Porada, Zhao, van der Wal, et al., 2013). In the adsorption cycle, the applied bias can be constant voltage (Dykstra et al., 2018; Kang et al., 2014; Qu et

al., 2016), constant current (Dykstra et al., 2018; Kang et al., 2014; Qu et al., 2016), or arbitrary voltage or current functions (Ramachandran et al., 2018). The CDI cell was discharged after the adsorption cycle, resulting in a high-salinity brine solution. Remarkably, a short circuit (0 V) was the most frequently used CDI discharge technique (Jande & Kim, 2013; Li & Zou, 2011; R. Zhao et al., 2013).

Several researches have pointed the appropriateness of CDI for mineral and metal recovery. The recovery of copper, nickel, chromium, phosphorus, and nitrogen from municipal wastewaters has been identified as one of the most promising applications in most CDI research. According to (C. Wang et al., 2019), CDI can be used to extract Cu^{2+}, Cr^{2+}, and Ni^{2+} from wastewater with good selectivity over NaCl and natural organic matter (NOM) in a competitive environment. Using CDI, research on lithium recovery demonstrates excellent removal efficiency, faster adsorption and desorption than traditional lithium recovery methods, and long-term durability. Over the last decade, several researchers performed research on fuel cells (Changchien et al., 2010; Nymand & Andersen, 2010), thermoelectric generators (Win et al., 2011), and solar cells (Dondi et al., 2008; Kobayashi et al., 2006) to collect electricity from lower power gadgets by utilizing DC/DC converter.

The energy accumulated in the EDL might be transferable into a supercapacitor (SC) or battery, which makes the CDI system a good option for energy recovery using a DC/DC converter. The energy recovery mechanism offers an opportunity for the CDI system to enhance the overall performance of desalination. Several attempts have been made to improve energy recovery efficiency from CDI systems (Alkuran et al., 2008a; L. Chen et al., 2018; Kang et al., 2016a; Pernia et al., 2014). Kang et al. (2016b) used a buck-boost converter to demonstrate energy recovery from the membrane CDI system to an SC.

1.2 Statement of the Problem

In 2003, (Długołęcki & Wal, 2013) published the first research on the concept of energy transfer mechanism in CDI cells. They calculated the theoretical recovered and consumed energy from the membrane capacitive deionization (mCDI) without practically recovering energy (Długołęcki & Wal, 2013; García-Quismondo et al., 2013; Jeon et al., 2014. On the other hand, Pernia and Alkuran et al. proposed a DC-DC converter-based energy recovery mechanism form the CDI desalination cell

(Alkuran et al., 2008b; Pernía et al., 2012). The authors used a buck-boost converter to control the energy transfer between the SC and CDI systems.

The recommended CDI system cannot explain the CDI's real desalination activity, which was a shortcoming of that research. Because of the discharge current restrictions, the energy recovery was decreased. The discharge current was uncontrolled in the Shunt case because the mCDI system was short-circuited, and the salt was circulated in the same solution within a brief period, while the energy collected in the electrodes was wasted as heat inside the electrodes and external circuits.

Traditional heavy metal recovery methods, such as coagulation-flocculation and chemical precipitation, struggle to remove heavy metals selectively and produce huge amounts of harmful solid sludge. Desalination processes can theoretically be used to remove heavy metal ions; however, they may become inefficient since heavy metal contamination occurs at considerably lower concentrations than usual salts. Electrosorption procedures are developing as an efficient and simple way to remove heavy metals and other ions from water. In this thesis, metal recovery was performed from the CDI desorption metal solution. Heavy metal likes Cu^{2+}, Cr^{2+}, and Ni^{2+} are recovered in the form of electroplating on stainless steel. Initially to collect the CDI desorption solution and energy recovery, a simple CDI cell was constructed.

However, there has not been much research on activated carbon cloth (ACC) based CDI to remove various species of heavy metals, recovery, and energy recovery. The existing ones have either utilized complicated or expensive production techniques and materials. As a result, a study of the ACC-based CDI cell to explore the capability of various metal ions under varied voltages will be advantageous to CDI progress. In this thesis, buck-boost converter and supercapacitor-based energy recovery mechanisms was considered to recover the energy form the CDI cell. Primarily, the energy was transmitted to the buck-boost converter from the CDI desalination cell and then the temporarily stored energy in the inductor was transferred to the energy storage device—this type of energy recovery was considered as single-way energy transfer/recovery.

1.3 Objectives of the Study

The objective of the study was to develop a mechanism to recover selected metals from CDI discharged brine using an ACC-based CDI cell. Moreover, energy recovery from

the ion desorption phase via a buck-boost converter and its efficiency was also investigated. The specific objectives are as follows:

1. To fabricate and characterize an activated carbon cloth-based CDI cell.
2. To study the impact of applied voltage on various heavy metal recovery from the discharged brine of the ACC-based CDI cell.
3. To recover energy from the CDI system using buck-boost converter and supercapacitor.

1.4 Scope of the Study.

In this thesis, the potential for various types of heavy metals like (Copper (Cu^{2+}), Nickel (Ni^{2+}), and chromium (Cr^{3+})) recovery from the ACC-based CDI cell desorption solution was studied individually and compared with the existing literature. There is energy induced and stored in the electrode during the adsorption steps, subsequently, this energy become wasted. Hence, an energy recovery mechanism was developed to recover energy from the ACC-based CDI cell by utilizing a buck-boost converter and supercapacitor. To perform the energy recovery and metal recovery, a CDI cell was constructed. Furthermore, the performance of the developed energy recovery system connected to the CDI cell was evaluated and compared with the existing energy recovery techniques.

1.5 Limitations of the Study

- Only copper (Cu^{2+}), nickel (Ni^{2+}), and chromium (Cr^{3+}) ions are investigated for the metal recovery using the ACC-based CDI cell desorption solution.
- Only buck-boost converter-dependent mechanism was utilized to recover the energy from the ACC-based CDI systems. Moreover, the converter bought whose rating was not similar to our requirement. Hence, we used amplifier, voltage comparator, and voltage divider circuit, which affected the outcome of the energy recovery efficiency.
- The study considered only ACC as the electrode material for the CDI system.

1.6 Organizations of the Report

This thesis is divided into five chapters which are planned as follows:

Chapter 1: 1st chapter includes the background of the study, statement of the problem, objectives, scopes of the study, limitations of this thesis, and the organization of the study.

Chapter 2: Various literature was reviewed in this chapter, which are related to energy and metal recovery using CDI technique. The existing energy recovery mechanisms for recovering the energy from the CDI, FCDI, MCDI, i-CDI, and i-MCDI cell; operating mechanism, configurations, advantages, and limitations; types of converters; energy transfers; types of energy storages for capacitive deionization are reviewed and discussed.

Chapter 3: Represent the construction of CDI cell; experimental mechanism of the activated carbon cloth (ACC) electrodes-based CDI cell with energy recovery system; operating principle of the proposed energy recovery technique; key performance indicators of the proposed energy recovery system; and the potential for various types of heavy metal recovery from the CDI desorption solution.

Chapter 4: This chapter discusses the results of the CDI cell operation to check the working behavior of the constructed CDI cell; the impact of different applied voltage and different pH on heavy metal recovery in the form of electroplating from the CDI discharged brine; and the energy recovery mechanism of the ACC-based CDI cell. The outcomes are compared with other existing energy recovery techniques.

Chapter 5: This chapter summarizes the findings of this thesis study and provides future research recommendations.

CHAPTER 2
LITERATURE REVIEW

2.1 Why Metal Recovery is Important?

With the rapid industrial revolution, industrial wastewater containing heavy metals was frequently dumped into the environment, either directly or indirectly, without treatment (Carvalho Barros et al., 2018). The majority of heavy metals like copper, nickel, cobalt, mercury, cadmium, lead, and chromium are an extremely hazardous and significant influence on human health and the environment. Copper (Cu^{2+}), nickel (Ni^{2+}), and chromium (Cr^{3+}) are hazardous contaminants, which produced in a variety of industries, including printing circuits, plating, metallurgy, and mining (Zhan et al., 2011). Cu^{2+} discharge into inland surface waters has a tolerance limit of 3.0 mg/L, while drinking water has a tolerance limit of 0.05 mg/L (Huang & Su, 2010). As a result, removing Cu^{2+} from the water was critical, and many technologies have been developed. Electrodialysis, ion exchange, reverse osmosis, distillation, and chemical precipitation (Z. Chen et al., 2015; Dehkhoda et al., 2016) are some of the traditional processes that have produced a substantial amount of cleaned water in recent years. These processes frequently come at a higher price, requiring large investments and a lot of energy (Z. Wang et al., 2012). Although much effort has been put into developing methods for purifying Cu^{2+}, Ni^{2+}, and Cr^{3+} containing effluents, less emphasis has been paid to recovering metallic copper, chromium, and nickel for sale or reuse. Apart from this, pristine MnO_2 has been widely used as one of the electrodes in CDI cells due to its electrochemical properties and high electrosorption capacity via ion intercalation. Its use as an anode greatly improved adsorption capacity and stability as it does not suffer from oxidation like carbon electrodes (Tan et al., 2020; Wu et al., 2018). However, its performance was limited by its low conductivity (Lin et al., 2018).

2.2 Conventional Heavy Metal and Energy Recovery Techniques

Even though heavy metal pollution was a major threat to both the human race and the environment, but the sources of the problem can be simply identified. Heavy metal at toxic concentrations was routinely found in wastewater released by industry; thus, heavy metal recovery techniques can easily be included in the water treatment process to eliminate the problem. Heavy metal recovery from industrial wastewater can be

accomplished using a wide variety of methods such as ion exchange, precipitation, adsorption techniques, membrane filtration, and other procedures (Almomani et al., 2020). Each method has its own set of benefits and compatibility with various water treatment settings. Most of these strategies still have limitations restricting their long-term effectiveness as continued water desalination (Ajao et al., 2020; C. Liu et al., 2019; Qasem et al., 2021).

Electroplating was the most frequently used metal recovery technique for industrial wastewater. Electroplating process started in 1996 to recover the heavy metal (Armstrong et al., 1996). (Li et al., 2011) introduced a novel metal recovery technique, which was the combination of acid-leaching and electroplating to recover metal. The authors showed that up to 95% of the metal could be extracted after 12 hours of treatment. (Min et al., 2019) investigated the electrodialysis approach to separate the heavy metal from the wastewater. The authors show that the deposition rate was increasing along with the increment of concentration range. Moreover, authors demonstrated that electrodialysis could recover more than 90% of metals from the electroplating wastewater. (Nepel et al., 2020) shows that around 82% copper can be recovered from the real jewelry wastewater using kinetic determination and fast galvanic pulse electrochemical approaches. Here, to see the distribution and morphology, the authors performed scanning electron microscopy (SEM), energy-dispersive X-ray detector (EDX), and X-ray photoelectron spectroscopy (XPS). (Chen et al., 2013) developed a hybrid approach based on electrolysis and electrodialysis to extract copper from the wastewater. The authors revealed that around 82% of copper was recovered from the highly concentrated wastewater (greater than 400 mg/L). (Peng et al., 2011) performed copper recovery from industrial wastewater in the form of electro treatment using a titanium (Ti) coated reactor. The authors utilized constant current during the metallic copper recovery. Moreover, the authors revealed that the recovery efficiency was around 99.9%.

The rising need for energy and water has been a serious global problem due to fast population growth and technological progress. Hence, in recent years, the interdependence of energy and water has been a vital concern (DeNooyer et al., 2016; Fang & Chen, 2017; Shang et al., 2018). There are two types of energy recovery mechanisms: a) direct energy recovery and b) converter-based energy recovery.

Table 2.1

Comparison Among Existing Heavy Metal and Energy Recovery Techniques

Authors and Ref.	Recovery Types	Electrode Types	Efficiency	Limitation/ Research gap
(C. Wang et al., 2019)	Metal recovery: MCDI	activated carbon fiber	42.8%	Electrode regeneration efficiency is lower
(Kim et al., 2017)	Metal recovery: MCDI	Carbon Electrodes	99.07-99.94%	0.17% decrease in Pd removal for every cycle
(P. Liu et al., 2017)	Heavy metals and salty ions: CDI	3D graphene-based asymmetric electrodes	98.7%	Construction is complicated
(Y. W. Chen et al., 2019)	Energy Recovery: CDI	activated carbon electrode	49.6%	-
(Jeon et al., 2014)	Energy Recovery: FCDI	flow-electrodes	20% of supplied energy	-
(Rommerskirchen et al., 2018)	Energy Recovery: FCDI	flow-electrodes	36% of supplied energy	Electrode losses not included
(Omosebi et al., 2020)	Energy Recovery: i-CDI, i-MCDI	Porous electrodes	energy penalty reduced to ∼8 and 4 J g^{-1} for i-CDI and i-MCDI, respectively	The outcome may further be extended by reducing charge leakage
(Oyarzun et al., 2020)	Energy Recovery: CDI	activated carbon porous electrodes	90% for an initial voltage of 1 V	Overall system efficiencies are significantly lower than the storage and utilization efficiencies
(Tan et al., 2020)	Energy Recovery: MCDI	mCDI electrode	40% of the supplied	Careful selection of high-current contacts and conductors may further increase the energy recovery
(Ma et al., 2019)	Energy Recovery: FCDI	flow-electrodes	60%	-
(L. Chen et al., 2018)	Energy Recovery: MCDI	activated carbon fiber	46.6%	Further energy recovery can be improved by decreasing resistance in the MCDI stack electrode

2.2.1 Adsorption-based Metal Recovery

The adsorption technique has long been utilized in water treatment, still significant interest in further development because of its numerous advantages, including simplicity, low cost, re-usability, and design and modification flexibility (Chang et al., 2020). Adsorption capability for selective removal of certain chemicals, such as organic components, polymers, and heavy metal ions, has also been studied in numerous studies. Adsorption works by exposing the adsorbent to industrial wastewater and allowing the metal ions to be adsorbed. Adsorption systems come in a variety of designs and configurations due to the process's simplicity. Heat, chemical agents, and other ways can all be used to regenerate the adsorbents. However, the dependency on chemical agents or energy loss during heat regeneration was considered as the disadvantage of this process (Demirbas, 2008; Vakili et al., 2019).

Based on the literature, the traditional procedures were frequently constrained by a large reliance on chemical agents, high operational costs, high energy consumption, or complex system design. Even though their efficiency in removing a heavy metal may only be feasible for small solutions. Because many of their flaws might lead to long-term environmental issues, employing the strategies may become obsolete when the process becomes a secondary source of the environmental problems. As a result, heavy metal removal approaches must be investigated to provide a better metal recovery rate and efficiency while avoiding the same drawbacks.

2.2.2 Membrane-based Metal Recovery

Membrane-based technology was another widely utilized water treatment process. These techniques are commonly used in the industrial wastewater treatment sector because of their efficiency and ability to separate a broad range of contaminants, from dissolved organic and inorganic compounds to solid particles and bacteria. The membrane-based process utilizes the membrane. The membrane is a physical barrier that permits ions' flow (Ritchie & Bhattacharyya, 2002; F. Zhao et al., 2020). The membrane can remove substances through a variety of methods, including size exclusion, ion charges, and interactions with the membranes themselves.

This technique was used for heavy metal recovery and whole-water treatment. A water treatment system was frequently constructed using the membrane process as the primary contributor to obtaining the desired treated water qualities due to its removal

efficiency. Feedwater must be conditioned by various pretreatments to enhance its performance and protect the membrane. Post-treatments are also necessary to stabilize the treated water within reusable or releasable conditions. As a result, the membrane process was not commonly used for heavy metal recovery due to its high capital and operational costs associated with its implementation.

2.2.3 Direct Energy Recovery

Direct energy recovery was the mechanism to harvest energy from the CDI cell without external mechanisms. (Ma et al., 2019), introduced a novel flow-electrode CDI (FCDI) mechanism to recover energy using a two-chamber device. In this technique, with constant current, the adsorbed electrodes are discharged. The authors also demonstrate that a single constant discharge current can achieve the maximum energy of 36.3 J at 0.50 mA/cm2. Moreover, more energy was recovered with the help of successive discharge currents. Furthermore, by utilizing extra carbon nanotubes as conductive agents in the electrodes, the outcome was additionally improved by 60%. Another study by (Jeon et al., 2014) proposed an FCDI cell for energy recovery and ion storage. Here authors charge the flow-electrode by constant voltage, producing around 20% of the input energy in the FCDI system during constant current discharge. (Rommerskirchen et al., 2018), introduced a continuous FCDI process to recover energy. In this work, the authors illustrate that up to 36% of applied energy can be recovered during the regeneration of electrodes in the desalination cycle.

(Y. W. Chen et al., 2019) proposed a novel membrane capacitive deionization (MCDI) cell to distinguish the impacts of charging/discharging current and voltage on electrode regeneration and energy recovery. The authors show that, by varying the constant voltage and current, the energy recovery ratio was varied as well. Furthermore, the investigation of the electrode's regeneration illustrated that both in constant current and voltage mode, the regeneration ratio increased with the decreasing discharge current. Finally, they found that the regeneration of electrodes was approximately 64% in CV and 86% in CC mode at the discharging current of 0.1 A.

2.2.4 Converter-Based Energy Recovery

Converter-based energy recovery was the mechanism to harvest energy from the CDI cell with the help of external energy storage and dc-dc converter. (Chen et al., 2019) constructed a novel mechanism to transfer the electric energy from the CDI cell by

utilizing a supercapacitor and four-switch buck-boost converter. The proposed mechanism was divided into two stages: energy recovery and ion removal by stop-flow operation during the charging stage, and electrode regeneration was performed during the discharging stage. The authors illustrate that the recovered energy rate was accomplished by reducing the distance between electrodes and greater inflowing NaCl concentrations. Additionally, they found that the energy recovery ratio in the CDI cell was increased up to 49.6%, while the salinity was reduced to 50 mM NaCl solution. (Oyarzun et al., 2020) proposed a novel closed-form analytical approach between buck-boost converter and supercapacitor to increase the energy transfer efficiency. In this model, the authors use a one-way storage mode and both-way utilization mode in between energy storage and CDI cell by utilizing a simple DC/DC converter circuit. The proposed approach ensured the utilization efficiency was around 90% at the initial voltage of 1V. Moreover, the authors guide the selection of parameters to maximize the energy transfer ratio. (Pernía et al., 2012) introduced a novel energy recovery technique along with water desalination by using an ordinary dc/dc converter in the CDI cell. The step-by-step energy recovery process and characteristics of the CDI cell were investigated. They designed an up/down converter to recover the energy from the CDI cell more effectively. (Pernia et al., 2014) investigated an electric approach to describe various energy loss parameters in the converter and CDI cell to build more efficient CDI cells. (Pernia et al., 2014) designed a novel CDI cell to analyze its characteristics and performances by solving the differential equation that represents the behavior of the entire CDI cell. The differential equation provided an idea about the most optimal current for charging the CDI cell and the optimal energy recovery efficiency. According to the comparison of theoretical outcome and experimental outcome, it's clear that theoretical prediction was better than the experimental outcome in the developed CDI cell. The authors used the following equation to calculate energy loss:

$$E_{R_{S_j}} = R_S \cdot \left[\int_0^{t_{ON_j}} i_{L_{ON_j}}^2(t)dt + \int_0^{t_{OFF_j}} i_{L_{OFF_j}}^2(t)dt \right] \qquad (2.1)$$

$$E_{R_{P_j}} = \frac{1}{R_P} \cdot \left[\int_0^{t_{ON_j}} \left(V_{C1_{ON_j}}^2(t) + V_{C2_{ON_j}}^2(t) \right) dt + \int_0^{t_{OFF_j}} \left(V_{C1_{OFF_j}}^2(t) + V_{C2_{OFF_j}}^2(t) \right) dt \right] \qquad (2.2)$$

Moreover, the net energy loss by leaking in R_P and conduction R_S from C_1 to C_2 is found by the summation of all cycle contributions. That was calculated as follows:

$$E_{TotalLoss} = \sum_{j=1}^{j=n} \left[E_{R_{S_j}} + E_{R_{P_j}} \right] \quad (2.3)$$

(Tan et al., 2020) introduced a novel energy recovery strategy using mCDI cells from brackish water by utilizing bi-directional dc-dc converters. This approach was also applied in a pilot-scale prototype and assessed its performance. The authors demonstrated that the pilot-scale mCDI unit could reduce energy consumption by using an energy recovery mechanism with the combination of photovoltaic energy and battery storage by 30 to 40%. Moreover, the stop-flow operation can increase water recovery by around 87%. (Kang et al., 2016b) developed a novel direct energy recovery process using the mCDI cell under different conditions by utilizing a supercapacitor as energy storage and buck-boost converter. Based on the outcome, the higher constant charging voltage (CV) and longer charging time ensured a higher energy recovery rate. The outcome of this article ensured that constant current charging and the amount of salt adsorption play a vital role in the energy recovery system.

(Omosebi et al., 2020) introduced a new energy recovery approach from one inverted CDI (i-CDI) cell by utilizing a Ćuk converter. In this experiment authors used two cells; hence the charge stored during the desorption stage was transferred to another CDI cell during the charge step. The overall energy consumption for water desalination in the CDI cell can be reduced by following this way. Based on the outcome of this strategy, the energy loss can decrease by up to 8 J g−1 and 4 J g−1 for i-CDI and i-MCDI modules, respectively. Furthermore, i-MCDI demonstrates up to 3 times higher leakage resistance than the i-CDI cell by simply reducing the leakage charge.

2.3 Energy Transfer

Energy transfer was another vital parameter in the energy recovery mechanism. Energy transfer also depends on various parameters. The energy transfer was performed in the desorption steps. According to (Jeon et al., 2014), the amount of charge transfer during the desorption steps can be obtained by integrating the current measured. Figure 2.1 represents the input energy and recovered energy ratio during the charging and discharging steps, respectively. The recovered energy W(Wh) during the discharging

process can be obtained by integrating the power over time. The net amount of supplied energy during the charging step was expressed by the following equation:

$$W_{charge} = V_{applied} \times \int_{t_i}^{t_f} Idt \qquad (2.4)$$

Where $V_{applied}$ represents the applied voltage during the charging step and I for current.

And the recovered energy during the discharging steps can be calculated by the following equation:

$$W_{discharge} = I_d \times \int_{t_i}^{t_f} V_{cell} dt \qquad (2.5)$$

Where I_d stands for the discharging current and V_{cell} represents the cell voltage.

(Omosebi et al., 2020), explained the way to evaluate the recovered energy from the i-CDI and i-MCDI cell using the Ćuk dc-dc converter. To evaluate the energy recovery efficiency, it was mandatory to charge the CDI cell with and without recovery steps. Hence, the fractional energy recovery (R) can be explained as follows: the amount of ionic charge recovered is defined by the difference of supply energy to the cell with and without the recovery process, divided by the total energy without the energy recovery process.

$$r = \frac{E_{PS|\text{No Recovery}} - E_{PS|\text{Recovery}}}{E_{PS|\text{No Recovery}}} \qquad (2.6)$$

(Oyarzun et al., 2020) introduced a novel technique to store the energy in the desorption cycle from CDI cells to store and reuse the stored energy in the subsequent adsorption cycle. The energy utilization efficiency is expressed following equation:

$$\eta_{util} = \frac{E_{CDI,rec}}{E_{out,CDI}} = \frac{E_{CDI,rec}}{E_{CDI,rec} + 2E_{L,DC-DC} + E_{L,ES,ch} + E_{L,ES,dis}} \qquad (2.7)$$

According to (Tan et al., 2020), Energy consumption (E) is expressed as follows:

$$E = \int_{t_1}^{t_2} u(t) \square i(t) dt \qquad (2.8)$$

Where, t_1 and t_2 stands for the starting time and ending times of certain stages, respectively. Whereas $u(t)$ and $i(t)$ represents the terminal voltage and input current, respectively. The authors utilized the oscilloscope to calculate energy consumption (E).

Figure 2.1

Input and Recovered Energy During the Charging and Discharging Stages, Respectively, and Their Ratio (Jeon et al., 2014b).

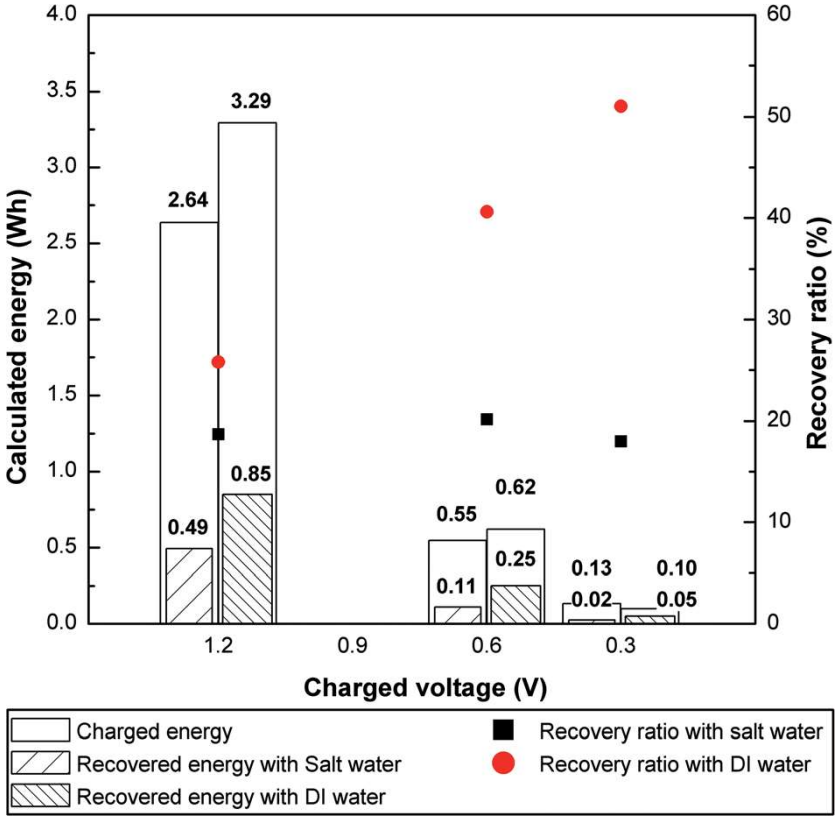

The average converter efficiency is expressed as follows:

$$\eta = \frac{E_{out}}{E_{in}} \qquad (2.9)$$

Where, E_{in} and E_{out} stands for the input and output energies in the bi-directional converter at the input and output terminal over a specified period. Based on this efficiency, the overall energy recovery performance can be assessed.

The voltage conversion rate of the bi-directional converter can be expressed as follows:

$$Voltage\ conversion\ ratio = \frac{V_{out}}{V_{in}} \qquad (2.10)$$

Where, V_{in} and V_{out} represent the converter's input voltage and output voltage, respectively.

2.4 Energy Storage from CDI Cell

Energy storage plays a crucial role in the energy recovery mechanism to enhance the overall performance of the CDI cell. There are different types of storage mechanisms utilized in the energy recovery mechanism from the CDI cell. The widely utilized storage techniques are as follows: one CDI cell to another CDI cell, Supercapacitor, and other types of energy storage devices. Based on the multiple literatures, all techniques contain their unique advantages over others. (Omosebi et al., 2020) did not utilize any kind of external storage device to recover the energy from the i-CDI and i-MCDI cell using Ćuk dc-dc converter. (Rommerskirchen et al., 2018) used two chambers and three-chamber modules to recover the energy from FCDI without using a converter and energy storage. (Jeon et al., 2014) also utilized the same mechanism to recover the energy and ion storage from the FCDI cell. (Chen et al., 2019) utilized six pairs of electrodes to recover the energy and electrode regeneration from the MCDI cell without requiring a converter and supercapacitor. (Ma et al., 2019) designed a three-chambered-based FCDI cell to recover the energy. The authors did not utilize any external energy recovery devices like converters, supercapacitors, or other energy storage devices.

(Kang et al., 2016b; Oyarzun et al., 2020; Pernía et al., 2012; Pernia et al., 2014) used up-down DC/DC converter and supercapacitors to recover the energy from the CDI cell. (Tan et al., 2020) utilized bidirectional dc-dc converter and battery storage to recover the energy from the mCDI cell. (Chen et al., 2019) utilized a four-switch buck-boost converter and supercapacitor for direct energy recovery from the desalination of brackish water.

CHAPTER 3
METHODOLOGY

3.1 Fabrication of the CDI Cell

3.1.1 CDI Electrode Preparation

Commercially available woven activated carbon cloth (Zorflex FM-100, USA) with a thickness of 1 mm and specific surface area of ~ 1200 m^2/g have been utilized as the primary carbon substrates. Firstly, the activated carbon cloths were immersed in 2 M HCl at 110 ºC for 12 hours in a vacuum oven. Then, thoroughly washed with DI water. Cleaned clothes were dried at 80 ºC in a vacuum oven for another 12 hours. Initially, we prepared the CDI cell using plain ACC, but the outcome of the ACC CDI cell was not satisfactory, which is shown in Section 4.1.1. Therefore, we have modified the plain ACC with the MnO_2, where 0.1 M $MnSO_4 \cdot H_2O$ and 0.1 M Na_2SO_4 in DI water were used as a precursor and a supporting electrolyte, respectively, for the deposition as a MnO_2 on the ACC surface. Figure 3.1 shows the fabrication of the ACC-MnO_2 electrode setup. To ensure uniform deposition of MnO_2, the ACC was put under a vacuum oven in the solution to remove trapped air inside the ACC pores. The deposition was carried out at room temperature and at controlled pH of 5.6. Then, the electrodes were dried in an oven overnight at 80 °C. Before every use, the cloth was degassed in the vacuum oven for around 15 minutes to enhance the absorption efficiency.

Figure 3.1

Fabrication of ACC-MnO2 Electrode Setup.

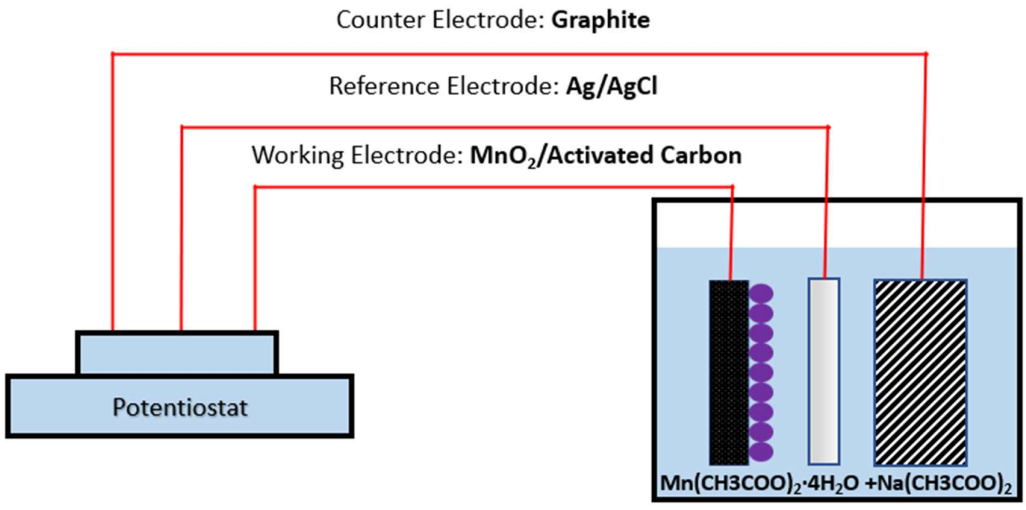

3.1.2 Characterization of the Fabricated Electrodes

The Scanning Electron Microscope (SEM, JEOL JSM7800F, JAPAN) was performed to examine the surface morphology to ensure the deposition of MnO_2, where the SEM was operated at an accelerating voltage of 2 kV and the magnification varied between x1,000-x10,000. Furthermore, the crystal structure was examined using X-ray powder diffraction (XRD, Rigaku TTRAX III, 50kV, 300mA, Cu/K_α, 1.54059Å), where the XRD outcomes were recorded between 10°-70°(2θ) with a scan step size of 0.02°.

The cyclic voltammetry (CV) electrodeposition was done using a potentiostat (Ossila™ potentiostat) to study the capacitive behavior and calculate the specific capacitance of the fabricated electrodes. A three-electrode cell with a 0.1M Na_2SO_4 electrolyte solution was used, where the platinum wire was used as a counter electrode and the Ag/AgCl electrode as the reference electrode. The voltammogram was recorded within the potential window of 0-1.0 V at multiple scan rates: 10 - 25 mV s^{-1}. The specific capacitances and areal capacitance from the CV curve were calculated using the following equations:

$$C_{specific} = \frac{\int_{V_a}^{V_c} IdV}{2mv(V_c - V_a)} \qquad (3.1)$$

$$C_{Areal} = \frac{\int_{V_a}^{V_c} IdV}{2Av(V_c - V_a)} \quad (3.2)$$

where, $C_{Specific}$ stands for specific capacitance, C_{Areal} for areal capacitance, V_c and V_a for the high and low potential limits of the CV tests, I for the instant current, m for the mass of the electrode, v for the potential scan rate, and A for the geometric area of the electrode.

3.1.3 Assembly of CDI Cell

A 4 cm x 4 cm CDI cell was constructed by stacking two ACC electrodes, two graphite foils, and a filter paper as the cathode, anode, current collector, and spacer within a gasket container shown in Figure 3.2. The acrylic plates were drilled with holes for water flow. After assembly, the cell was run with DI water until the conductivity of the water became stable.

Figure 3.2

Capacitive Deionization Cell Setup.

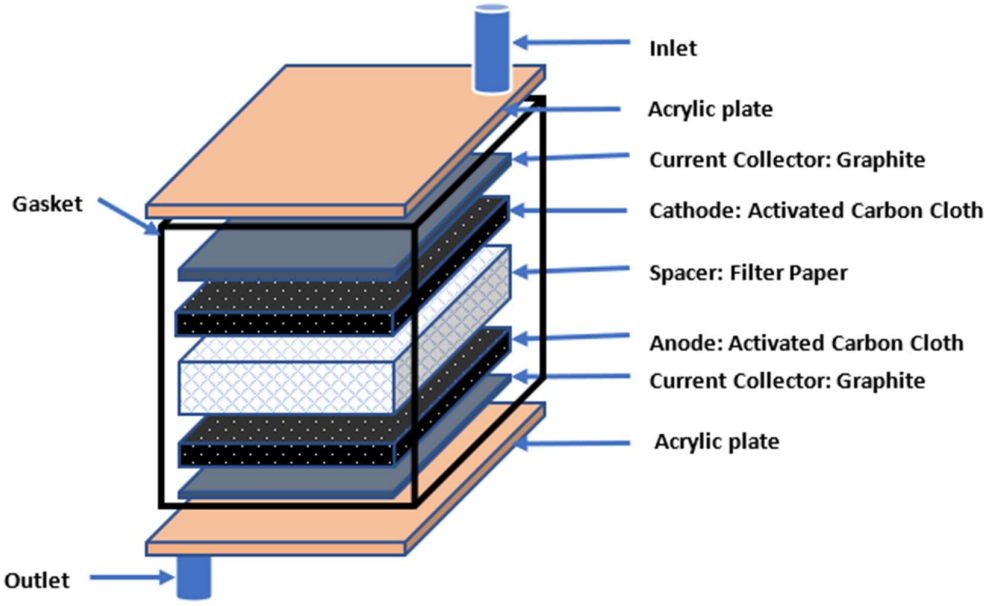

3.2 CDI Cell Performance Tests

3.2.1 Adsorption and Desorption Characteristics

To analyze the current of the adsorption and desorption cycle, sodium chloride (NaCl) solution was produced with DI water with a concentration of 1.5 mM. The CDI cell, the peristaltic pump, the solution tank, the DI water tank, two reservoirs, two power supply, and the data logger were used in a single flow mode, shown in Figure 3.3. The prepared NaCl solution was pumped through the system at approximately 10 mL/min for adsorption. CDI cell required a constant voltage below 1.2V to avoid breaking water. Therefore, the power supply provided a constant potential of 1.05V (Keithley 617 Programmable Electrometer). During the desorption cycle, PS 1 was turned off, and DI water was pumped through instead of the metal solution. The CDI system was connected in series with a resistor of 200 Ω to observe the voltage difference for the calculation of current. The current graph over time was studied for CDI adsorption and desorption characteristics. Figure 3.4 represents the ideal current and voltage behavior of the CDI. The current profile analysis was performed to ensure whether the CDI cell was working or not.

Figure 3.3

Data Collection and Solution Preparation Setup.

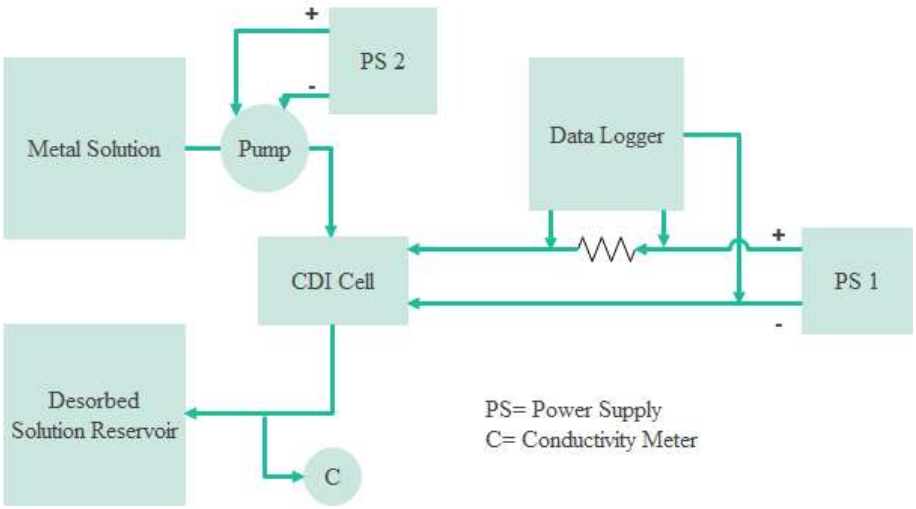

Figure 3.4

Ideal Adsorption and Desorption Behavior of CDI Cell

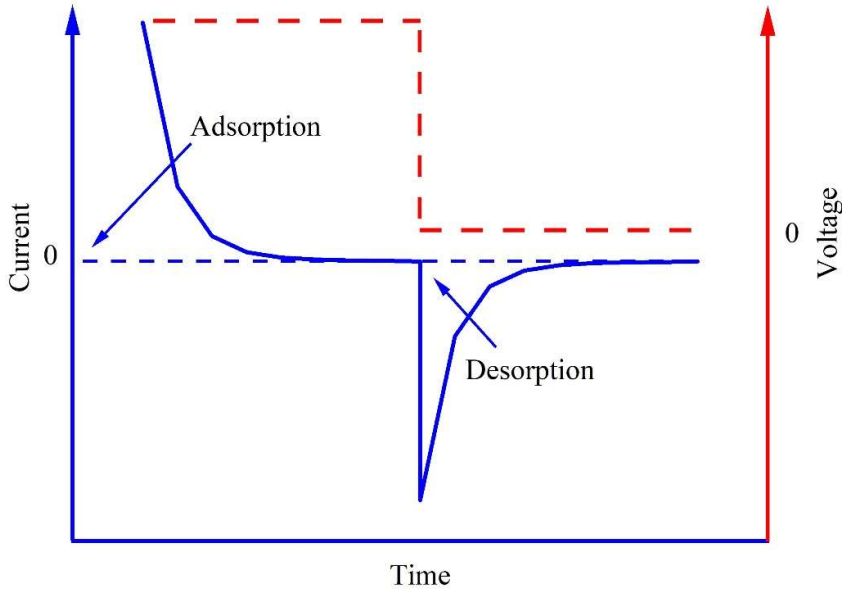

3.2.2 CDI Cell Performance Test Data Analysis

To analyze the performance of CDI cell, the salt adsorption capacity was calculated. The energy consumed by the peristaltic pump was not considered in this study. The following equation was used to calculate the salt adsorption capacity:

$$SAC(mg/g) = \frac{(C_o - C_t)V}{m} \quad (3.3)$$

Where, C_0 and C_t stands for the initial concentration and equilibrium concentration of ions (mg L^{-1}), respectively. m refers to the total mass of the two carbon electrodes when dry (g), and V represents the volume of NaCl solution (L). To calculate the current profile, the following equation was used:

$$I = \frac{V}{R} \quad (3.4)$$

where V represents the voltage difference across the CDI cell, and R stands for the resistor.

Integrated the area under the graph to get "total passed charges". Then the capacitance was obtained by dividing the total passed charges by the applied voltage, which is expressed as the following equations:

$$Total\ Passed\ charges = \sum(current \times time) \quad (3.5)$$

$$Capacitance = \frac{Total\ Passed\ charges}{Applied\ Voltage} \quad (3.6)$$

3.3 Metal Recovery

3.3.1 Preparation of Solution

Individual solutions containing the metal species like $Cu(NO_3)_2$, $Ni(NO_3)_2$, and $Cr(NO_3)_3$, were produced with DI water at the concentration of 0.5 and1.5 mM. This manually prepared solution is then run through the CDI cell to produce CDI discharged brine solution. Initially, during the adsorption phase, the pump circulates the solution from the solution tank through the CDI and is stored in the adsorbed reservoir. The CDI's output solution was stored in the desorbed reservoir during the desorption phase. In the second cycle, the manually prepared metal solution was used as the adsorbed solution; during the desorption cycle, the stored desorbed solution of 1st cycle was used as the input solution. Similarly, we followed this adsorption and desorption cycle for 5 times to get a more concentrated ion solution for metal recovery. The different ion concentration data after the adsorption and desorption cycle showed in Section 4.2.1. The flow rate and applied voltage was 10mL/min and 1.05V, respectively. The conductivity of the adsorbed and desorbed solution was checked to identify the

concentration change. The calibration curve of each metal species was prepared to determine the concentration during the desorption cycle, shown in Appendix A. The solution was collected for metal recovery in the form of electroplating. As the pH plays a critical role in the metal recovery performance. Hence, sulfuric acid (H_2SO_4) and boric acid (H_3BO_3) were used for pH adjustment in the solution.

3.3.2 Metal Recovery Setup

The experimental setup consists of two electrodes: AISI 304 stainless steel as cathode with the dimension of 2cm x 1cm, and the other electrode was graphite as anode with the dimension of 4.7cm x 2.7cm. The experiments were performed in a glass beaker. A power supply from the NICE-POWER company was used to supply the constant voltage in the metal recovery cell according to the metal requirements. Figure 3.5 represents the metal recovery setup using stainless steel and graphite electrodes from the regeneration solution.

Figure 3.5

A Schematic Representation of Metal Recovery Setup by Electroplating

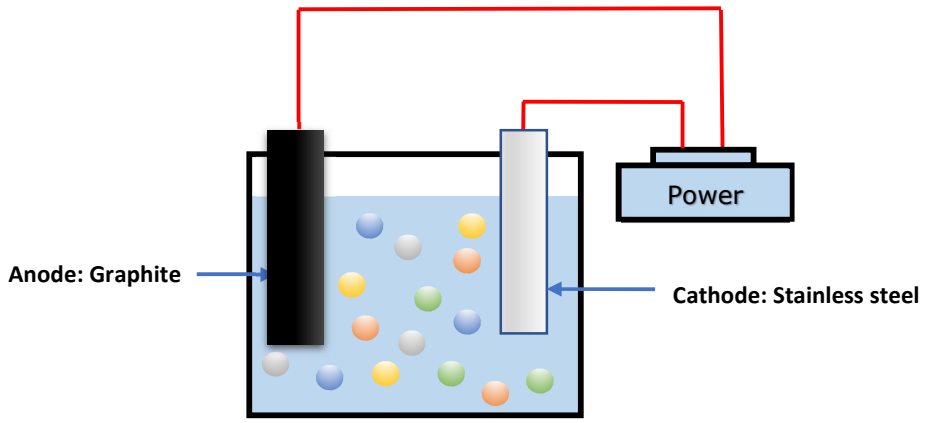

According to several literature (T.-C. Chen et al., 2013; P. P. Li et al., 2011; Peng et al., 2011), metal recovery in the form of electroplating was directly related to the applied voltage and pH value. To find out the optimum voltage and pH value to recover metal by utilizing less energy, the following conditions were varied during metal recovery:

Table 3.1

Name of the Parameters and Their Variations

Factor Name	Variation
Metal Ion Species	Cu^{2+}, Cr^{2+}, Ni^{2+}
Metal Ion Presence	Individually
Salt Concentration	0.5mM-1.5mM
pH	Copper= 1.90 -2.50
	Chromium= 2.40-3.50
	Nickel= 4.0
Applied Voltage	Copper= 1.5- 3.0V
	Chromium= 2.0-7.0V
	Nickel= 5.0 and 5.5V
Regeneration Cycle	1 Cycle and
	5 Cycle

3.3.3 Metal Recovery Substrate Preparation and Deposition Procedures

Before performing the metal recovery, the following pretreatment was done to ensure better deposition: initially, washed the stainless steel thoroughly with acetone for 30 minutes to clean the substrate. Then, thoroughly wash the steel with DI water before being kept in the 80^0C oven for 8 hours. Next, the metal deposition was performed on the stainless steel using the process shown in Figure 3.5. In every deposition, a 40mL new solution was used. Upon metal deposition, the sample was thoroughly washed with DI water to remove ions, which were not deposited. Subsequently, the metal deposited steel samples were baked in the 80^0C oven for 12 hours. Measured the weight of the sample 10 times before and after the metal deposition to compare with the theoretical outcome. Lastly, take the photos of every sample to show the physical outlook and compare it with the literature's sample. After the deposition, the graphite electrode was cleaned with HCl and baked in 60^0C oven for 8 hours before reuse/new deposition.

Deposited sample cleaning after electrodeposition for reuse the stainless steel. The cleaning steps were performed as follows: for copper deposited substrate, Nitric acid (HNO_3) was used to clean the substrate, with the ratio of 10 H_2O:1 HNO_3. For chromium and nickel, the metal deposited samples were cleaned with hydrochloric acid

(HCl) with the same ratio. After adding the acid, the samples were staired for around 1 hour to get rid of the metal from the steel. Then, the steel samples were thoroughly washed with DI water. Afterward, the washed samples were baked at 80^0C oven for 12 hours before reuse/new deposition.

3.3.4 Metal Recovery Performance Tests

In terms of metal recovery, the changes in the concentration of metal ions in the solution indicate the amount of metal deposited on the steel. The efficiency of metal recovery was calculated using two methods. Firstly, the mass was measured before and after metal deposition to get the actual metal deposition. Then, using the current profile and faradays law of electrochemistry, theoretical deposited mass was calculated (Yang et al. 2021). The effectiveness of metal recovery was analyzed by the following equations:

$$Q = \int_0^t I(\tau) d\tau \qquad (3.7)$$

$$m = \frac{Q}{F}\left(\frac{M}{v}\right) \qquad (3.8)$$

where F stands for the faraday constant, M represents the molar mass of the specific metal, and Q stands for the charges.

Secondly, the atomic absorption spectroscopy (AAS) test was performed to get the actual deposition data of metal by measuring the concentration before and after deposition. Here we used AA-7000 atomic absorption spectrophotometer by Shimadzu. During the AAS, five different concentrated solutions were used to prepare the calibration curve. For the calibration curve, each solution was measured three times to get more reliable data. The test samples were repeated two times. The specific wavelength used during the AAS for copper and chromium was 324.8nm and 357.8nm, respectively. After obtaining the AAS data, the metal recovery efficiency was calculated using the following equation:

$$ER\% = \frac{C_0 - C_t}{C_0} \times 100\% \qquad (3.9)$$

Where, C_0 and C_t stands for the initial concentration and equilibrium concentration of ions (mg L^{-1}), respectively.

3.4 Energy Recovery

3.4.1 Energy Recovery Setup

In this thesis, energy recovery was performed using the MnO_2-ACC electrodes-based CDI cell. A filter paper dictated the space among two oppositely charged carbon electrodes. The net resistance in the CDI cell was divided into 2 types: ionic and electronic resistance. Here, the movement of electrons in the current collector, wire, and interface between carbon electrodes and current collector was referred to as electronic resistance. Ionic resistances also indicate ions' movement via the spacer channels' pores and the carbon electrode. The spacer channels and the carbon electrode were strongly influenced by the electrode distance and the concentration of the input solution. Figure 3.6 represents the energy recovery setup from the CDI system using buck/boost converter and a supercapacitor (SC). A 4 switches buck/boost converter was used to recover electric energy stored in the CDI cell. In this thesis, an SC (30 F) was utilized as an energy storage medium due to the long cycling durations, higher cycles effectiveness, and quick reversible energy charging and discharging (González et al., 2016; Luo et al., 2015; G. Wang et al., 2012). Furthermore, the SC's capacitance value was significantly greater than the normal capacitors, as highlighted in (Aneke & Wang, 2016). A small capacitor (22nF) has been added parallel to the CDI cell to avoid a sudden fluctuation in the current passing.

Figure 3.6

A schematic Presentation of Energy Recovery Setup Using Buck-Boost Converter and SC.

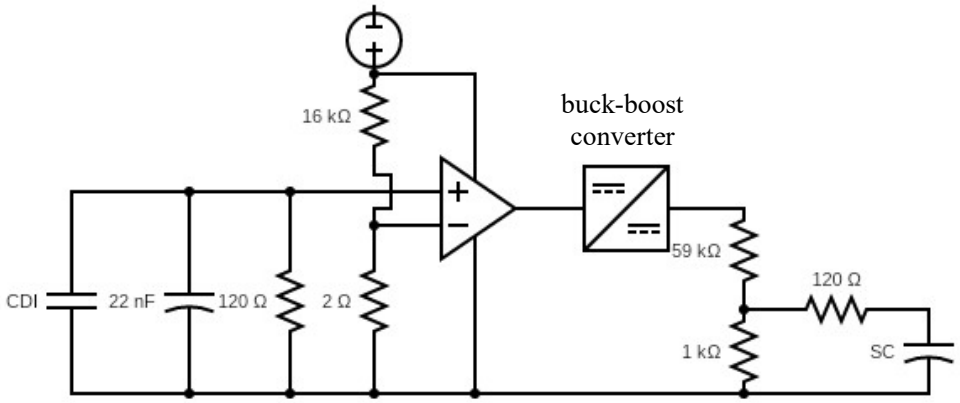

3.4.2 Energy Recovery Performance Tests

The entire mechanism was divided into two stages. Firstly, water desalination was performed during the charging phase. Then, energy recovery was performed by the designed circuit during the discharging cycle of the CDI cell. The energy recovery tests were performed in single-flow mode CDI cells. The solution was constantly pumped to the CDI cell with the 5 mL/min flow rate during the adsorption cycle to enhance the ion absorption. During the desorption cycle, 10 mL/min of DI water flowed to desorb the ion after energy recovery.

During the charging phase, the CDI cell was supplied with a constant supply of 1.05V. To calculate the energy recovery performance, the flow rate and the applied voltage were 5 mL/min and 1.05V, respectively. The energy recovery was performed using different metals like copper, chromium, and nickel to find out the impact of different metal. The charging time was also varied to identify the impact of the longer ion adsorption cycle. The CDI cell's response voltage fluctuation was measured continuously using a datalogger.

The CDI cell was immediately connected to the energy recovery circuit after the charging stage to transmit the stored electric energy from the electrode adsorbed ions to the SC. To improve the energy recovery efficiency, the pump was switched off for the entire energy transfer period, and the flow rate was reduced to zero. The stop/flow working mechanism was described by (Biesheuvel & van der Wal, 2010). After completing the energy recovery, the flow rate was 10 mL/min to desorb the ion with DI water.

3.4.3 Energy Recovery Performance Test Data Analysis

The energy recovery ratio was utilized to assess the effectiveness of the energy recovery from the CDI cell. The amount of charge transferred from the CDI cell to the SC was calculated by the equation shown in 3.7. The energy recovery efficiency was calculated using the following equation:

$$\varphi(\%) = \frac{\frac{1}{2} C_S V_S^2}{V_C \int_0^{t_c} I_C dt} \qquad (3.10)$$

Where, C_S stands for supercapacitor capacitance, V_S for supercapacitor voltage difference, V_C and I_C for the constant voltage and corresponding current during the CDI charging step.

CHAPTER 4
RESULT AND DISCUSSION

4.1 Fabrication and Characterization of CDI Cell

A 4 cm x 4 cm CDI cell was constructed by stacking two ACC electrodes, two graphite foils, and a filter paper as the anode, cathode, current collectors, and spacer within a gasket container. The acrylic plates were drilled with holes for water flow. The detailed construction of the CDI cell was described in Chapter 3 and its schematic diagram was shown in the Figure 3.2. Figure 4.1 represents the constructed CDI cell photographs, where (a) front and (b) side view of the cell is shown. In this section we discuss the adsorption and desorption characteristics of the CDI cell using current profile from the plain ACC electrodes and MnO_2 deposited ACC electrodes-based CDI cell and describe the working principle of the developed CDI cells.

Figure 4.1

Photographs of the Fabricated CDI Cell (a) Front View and (b) Side View

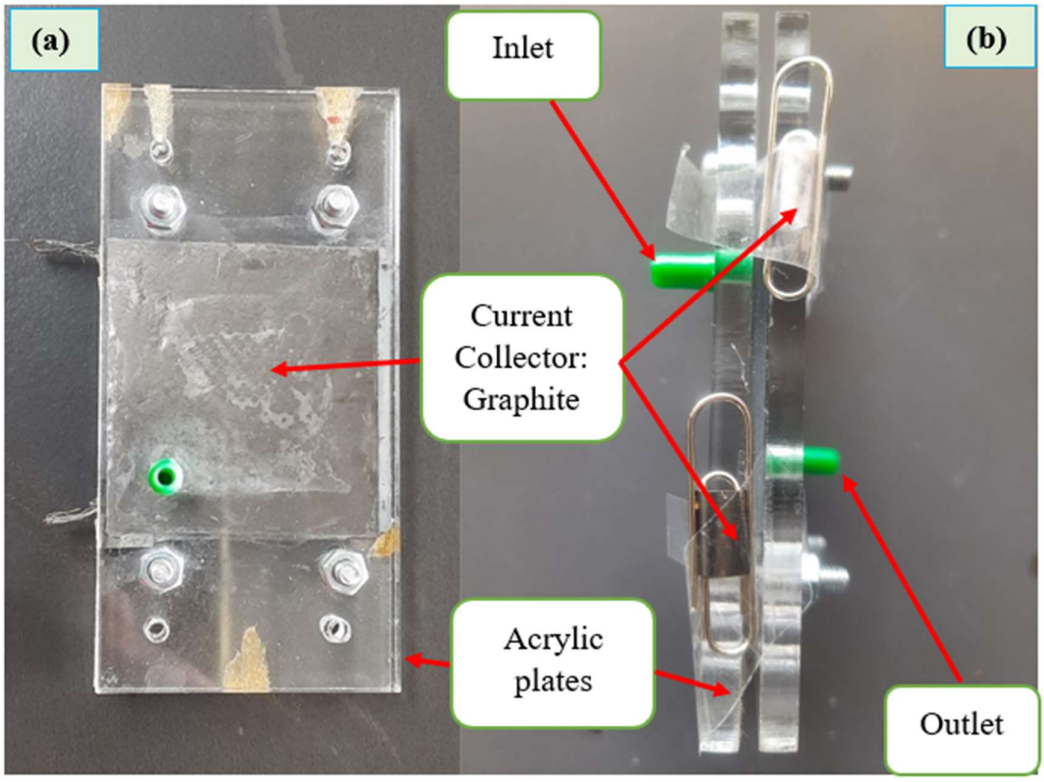

4.1.1 Adsorption and Desorption Characteristics of ACC based CDI Cell

To analyze the ion adsorption and desorption behavior of the CDI cell, we have recorded the current flowing through the cell during the adsorption and desorption cycles. Plain ACC electrodes were used as anode and cathodes during this experiment and a 2000 ppm NaCl aqueous solution was used to characterize the adsorption behavior of the cell. Figure 4.2 represents the adsorption and desorption current profiles of the CDI cell. During the adsorption cycle, as we applied the potential, the electrodes started absorbing ions. Positive ions were absorbed in the cathode. and negative ions in the anode. As the adsorption of ions continued, the current through the CDI cell started to drop which is similar to the charging behavior of a parallel plate capacitor where the charging current I_{ch} at any time t is given by $I_{ch} = I_0 e^{-t/\tau}$, where I_0 is the maximum value of the current flowing through the cell and τ is the time constant. Once the electrodes are saturated with adsorbed ions, the current stops flowing. On the other hand, during the desorption cycle, the applied potential across the electrodes of the CDI cell was kept zero and DI water was pass through the cell. Under this condition, the absorbed ions in the electrodes started releasing the ions to the DI water resulting in a gradual reduction in current approaching zero, similar to the discharging behavior of a parallel plate capacitor. The recorded current values showed a negative sign since the direction of the current flow is opposite during the desorption process.

Figure 4.2

CDI Current Profile Over Time representing (a) the Adsorption and (b) the Desorption Cycle of the Cell Recorded Using 2000 ppm NaCl Aqueous Solution.

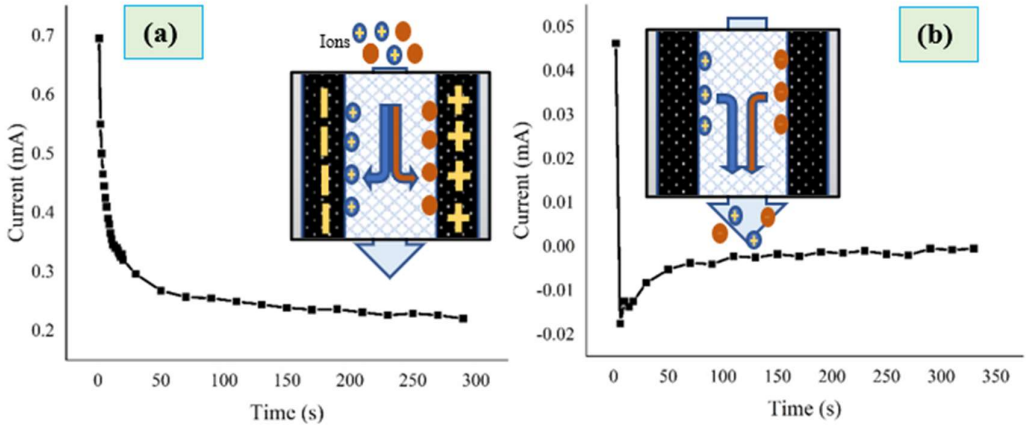

From the Figure 4.2 (a), it can be observed that the adsorption of NaCl in the plain ACC occurs within the first 100 seconds. Salt ions are mostly adsorbed in the pores of the ACC during this time. This adsorption happened quickly in the first 10 s resulting in a sharp drop (~50%) in the adsorption current. With time the adsorption process slowed down indicated by a slow change in the current. This happens since with the proceeding of the adsorption it become difficult for the salt ions to access the ACC pores. After 100 seconds, trivial change in the current was noticed. In terms of the desorption cycle, as shown in the Figure 4.2 (b) a similar behavior was observed. The desorption process mainly occurred in the first 100 seconds. The specific total passed charge using the plain ACC and 2000 ppm NaCl aq. solution was found around 161.53 mC/g of electrode. The detailed adsorption and desorption current values with respect to the time are given in the Appendix C.

4.1.2 Modification of ACC Electrodes with MnO_2

The adsorption capacity using plain ACC was lower. Therefore, to improve the adsorption capacity, the ACC electrodes were modified with the MnO_2. 0.1 M $MnSO_4 \cdot H_2O$ and 0.1 M Na_2SO_4 were used as the precursor and the supporting electrolyte, respectively for the deposition of MnO_2. Further, to ensure uniform deposition of MnO_2, the ACC were put under a vacuum while in the solution to remove air trapped within the pores of the ACC. These conditions were adopted from another ongoing research in our lab to deposit the MnO_2 on ACC surface. For the CDI cell characteristics, the applied voltage and NaCl solution flow rate conditions were kept similar as the case of the plain ACC electrode-based CDI cells. Figure 4.3 represents the adsorption and desorption current profiles for the MnO_2-ACC CDI cells recorded using the 2000 ppm NaCl solution. The plain ACC current over time data were replotted in the same figure for the comparison purpose.

The MnO_2-ACC CDI also showed similar adsorption and desorption behavior as in the case of the plain ACC CDI. The initial adsorption current for the MnO_2-ACC CDI was found to be almost 4.5 times higher than the plain ACC CDI cell indicating higher ion adsorption in the ACC electrodes after modification with MnO_2. The total passed charge with the MnO_2-ACC electrodes was found to be 1571.52 mC/g, which was significantly higher (more than 9 times) than the plain ACC electrodes. The salt adsorption capacity (SAC) for the MnO_2-ACC electrodes was found to be 14.25 mg/g,

compared to the SAC of 3.69 mg/g obtained for the plain ACC. The enhanced salt adsorption capacity of the MnO_2-ACC electrodes can be attributed mainly to two factors: (1) high areal capacitance and (2) enhanced surface area for ion adsorption following the deposition of the MnO_2 layers. In order to analyze these two factors, we carried out the cyclic voltammetry (CV) and scanning electron microscopy of the ACC and MnO_2-ACC electrodes, as shown in Figure 4.4. During the CV, the MnO_2-ACC electrode exhibited higher current density compared to the plain ACC indicating more ion adsorption capacity. This was also evident from the areal capacitance of the MnO_2-ACC electrode which was calculated as 134.51 mF/cm^2 compared to the 107.25 mF/cm^2 obtained for the plain ACC electrodes. SEM image in Figure 4.4 (b) showed deposition of MnO_2 on the ACC surface which will contribute to the enhanced surface area of the electrodes for ion adsorption.

Figure 4.3

MnO_2-ACC CDI Current Profiles Over Time Representing (a) the Adsorption and (b) the Desorption Cycles of the Cell Recorded Using 2000 ppm NaCl Aqueous Solution.

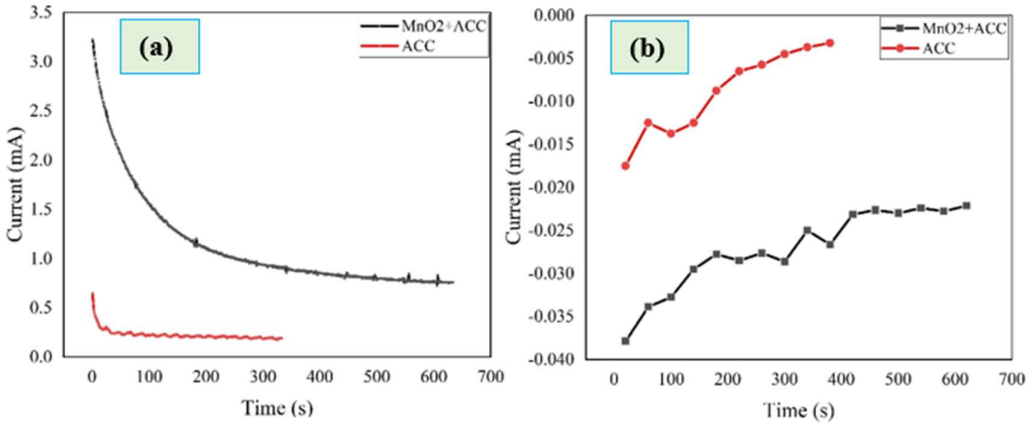

The adsorption of ions with the MnO_2-ACC electrode was also found to occur slowly compared to the plain ACC. The adsorption current was observed to gradually decrease up to about 300 s, after which it was saturated indicating very slow ion adsorption. Desorption current also exhibited a similar behavior and took almost 2 times longer time to desorb the ions compared to the plain ACC electrodes. This is because the MnO_2-ACC electrodes adsorb more ions compared to the plain ACC and the pores of the MnO_2-ACC electrodes are expected to be smaller than the plain ACC which makes it difficult for the ions to desorb and diffuse through the electrodes. The current at the end of the desorption cycle was also found slightly higher than the plain ACC electrodes

which is possibly an indication that some of the adsorbed ions in the MnO_2-ACC electrode remained permanently in the electrode due to the smaller pore sizes. However, this needs to be verified further and detailed BET analysis of the electrodes is required to analyze their pore size and volume distribution.

Figure 4.4

a) Cyclic Voltammetry of Plain ACC and MnO_2 Deposited ACC Electrode and b) SEM Image of MnO_2 Deposited ACC Electrode.

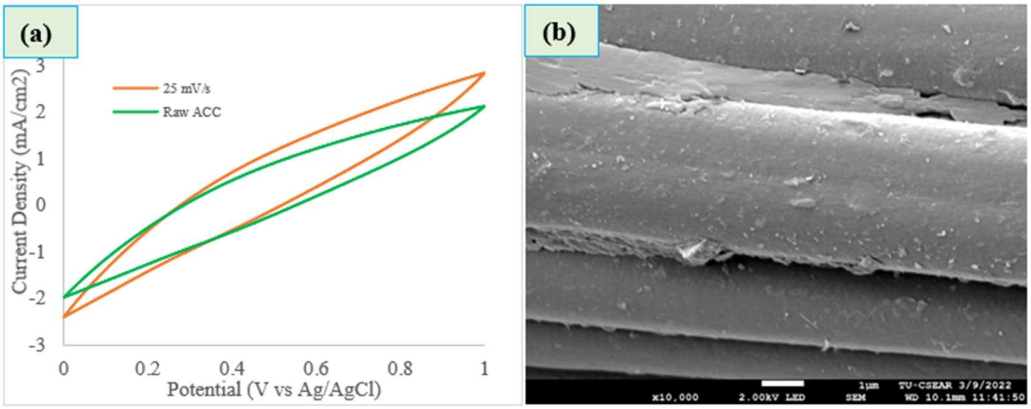

Based on these results we can say that the plain ACC-based electrode shows a quick adsorption and desorption time, which means the plain ACC could capture lower ions and release them quickly. On the other hand, the MnO_2-ACC electrode showed a longer adsorption and desorption cycle with higher salt adsorption capacity, but slower ion adsorption and desorption time. Due to the higher ion adsorption capacity, higher areal capacitance and higher surface area, we therefore decided to use the MnO_2-ACC electrode-based CDI system for the remaining studies.

4.2 Metal Recovery from CDI Effluent

This section discusses the impact of different applied voltage and pH on various heavy metal ion removal and recovery from the CDI effluent. In this thesis, the removal capability of Copper (Cu^{2+}), Nickel (Ni^{2+}), and Chromium (Cr^{2+}) ions and their recovery in the metallic form were examined. This section also discusses about the metal recovery efficiency. Some example current profile and specific current profile are added in the Appendix B. The current profile was very important for this experiment to calculate the energy efficiency using the Faradays law of electrochemistry. Lastly,

atomic absorption spectroscopy (AAS) test was performed to check the actual metal recovery efficiency after 1 hour of deposition.

4.2.1 Experimental Setup

Figure 4.6 represents the physical experimental metal recovery setup in the form of electroplating along with the data logger connection. This physical experimental setup was common for all the three types of metal which were recovered in this study. Figure 3.2 (b) represents the desorption solution collection process using CDI cell. Figure 3.6 represents the schematic representation of the Metal recovery setup by electroplating. Here, a datalogger was used to collect the voltage data across a 200-ohm resistance.

Figure 4.5

Metal Recovery Experimental Setup in the Form of Electroplating

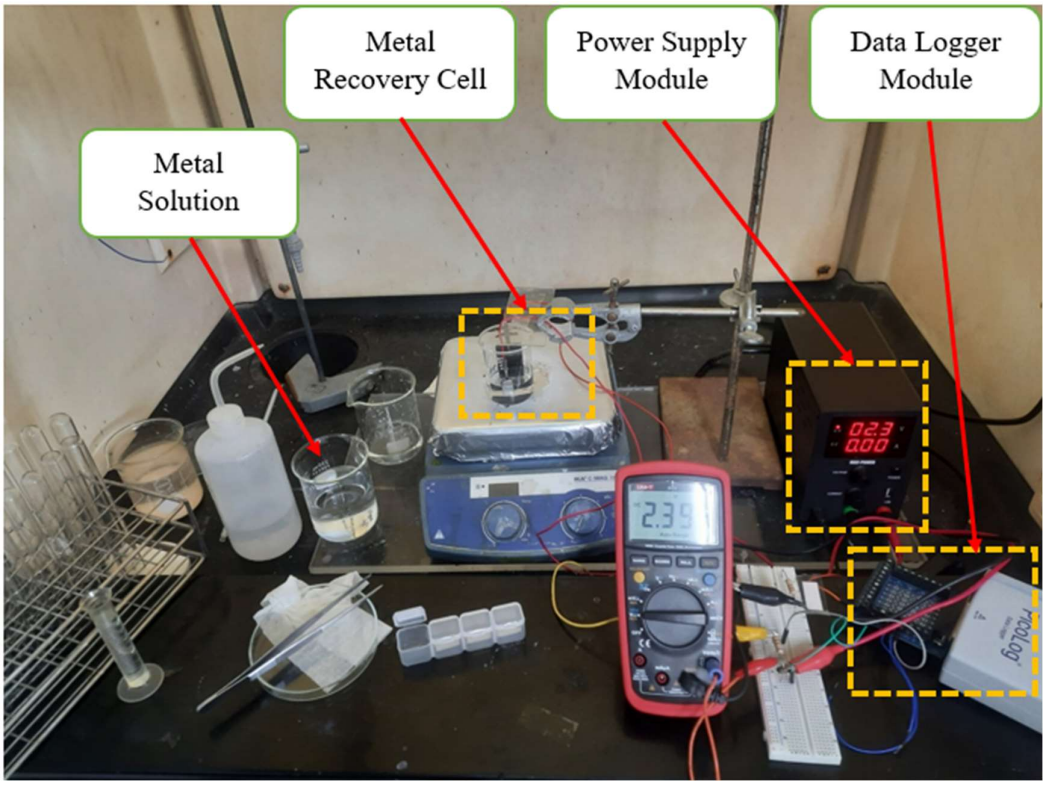

Copper, nickel, and chromium are most widely recovered metal from polluted water in the form of electroplating. In this thesis, to find out the appropriate voltage and pH value, a wide range of voltage and pH combinations were applied during the metal recovery. The pH for copper, chromium, and nickel were varied from 1.90 -2.50, 2.40-3.50, and 4.0, respectively. The applied voltage for copper, chromium, and nickel were

varied from 1.5-3.0V, 2.0-7.0V, and 5.0-5.5V, respectively. Two types of solutions were used to recover the metal. Firstly, the solutions were prepared manually by varying concertation. Here we mostly used 4 different concentration values like 0.5mM, 1.5mM, 1.6mM, and 3.0mM. Once the appropriate conditions were extracted, we used CDI effluent solution to recover the metal. The detail solution collection methodology described in the Section 3.4.

Figure 4.6 represents the different cycle and their corresponding adsorption and desorption current vs. time profile using 1.5mM copper and nickel solution, where the adsorption flow rate was 5 ml/min, and the desorption flow rate was 10 ml/min. During the desorption cycle, the reverse voltage was applied to ensure faster and complete desorption of the adsorbed ions. The graph of current over time has been studied for CDI adsorption characteristics.

Figure 4.6

Adsorption and Desorption Current vs. Time Profile Using a) Copper, and b) Nickel Ion Solution.

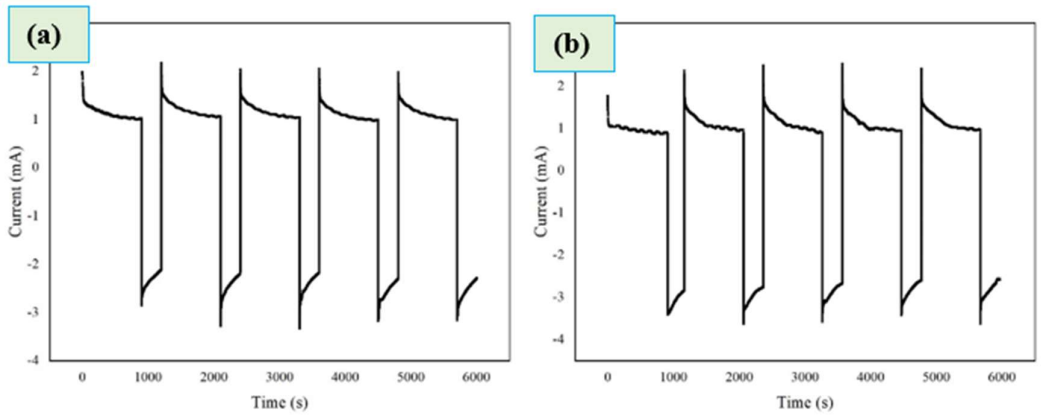

During the desorption solution preparation from the CDI cell, the concentration was measured using the conductivity meter. To measure the specific concentration after adsorption and desorption cycle, a calibration curve was prepared using the conductivity meter shown in the appendix A. Here the correlation coefficient was around 0.999. Table 4.1 represents the concentration of adsorption and desorption solution using copper, nickel, and chromium nitrate solution. Here the initial concentration was 1.5mM. From Table 4.1 it's clear that as the number of adsorption and desorption cycles increased, the concentration values were increased as well. But

the changes were very small compared to the time and energy because per cycle takes around 20 minutes of adsorption and 5 minutes (with reverse voltage) desorption cycle.

Table 4.1

Different Ion Concentration After Adsorption and Desorption Cycle.

Metal	**Copper ion concentration**		**Nickel ion concentration**		**Chromium ion concentration**	
No. of Cycle	Adsorption Concentration (mM)	Desorption Concentration (mM)	Adsorption Concentration (mM)	Desorption Concentration (mM)	Adsorption Concentration (mM)	Desorption Concentration (mM)
1	1.5	1.521	1.5	1.513	1.5	1.525
2	1.521	1.555	1.513	1.527	1.525	1.554
3	1.555	1.581	1.527	1.541	1.554	1.571
4	1.581	1.603	1.541	1.555	1.571	1.587
5	1.603	1.625	1.555	1.569	1.587	1.600

4.2.2 Effects of Applied Voltage on Different Metal Species Recovery

According to various literature, cell voltage plays the most important driving role in metal recovery in the form of electroplating.

4.2.2.1 Effects of Applied Voltage on Copper

The copper recovery was primarily performed with varying voltages like 1.5V, 1.7V, 2.0V, 2.5V, and 3.0V. For the initial experiment, 1000ppm copper nitrate solution was used to determine the appropriate voltage ranges. While we were looking for the appropriate applied voltage, we kept the pH fixed around ≈1.9. Figure 4.7: represents the copper deposited samples using different applied voltage. Some more copper deposited samples shown in the Appendix D.

Based on Figures 4.7 (e), the deposition rate increased with the increment of applied voltage. But at the applied voltage from 3.0V copper started forming copper oxide (CuO), which appeared as black color, shown in Figure 4.7 (a). Based on Figure 4.7 (b), the color of the first sample was different because mistakenly, we added sodium sulfate. The metal recovery current profile shown in Appendix B, where we noticed the current during copper recovery was higher. Due to sulfuric acid, the copper recovery draws more currents than other.

Figure 4.7

Stainless Steel After Copper Deposition at Different Applied Voltage and Deposition Trend.

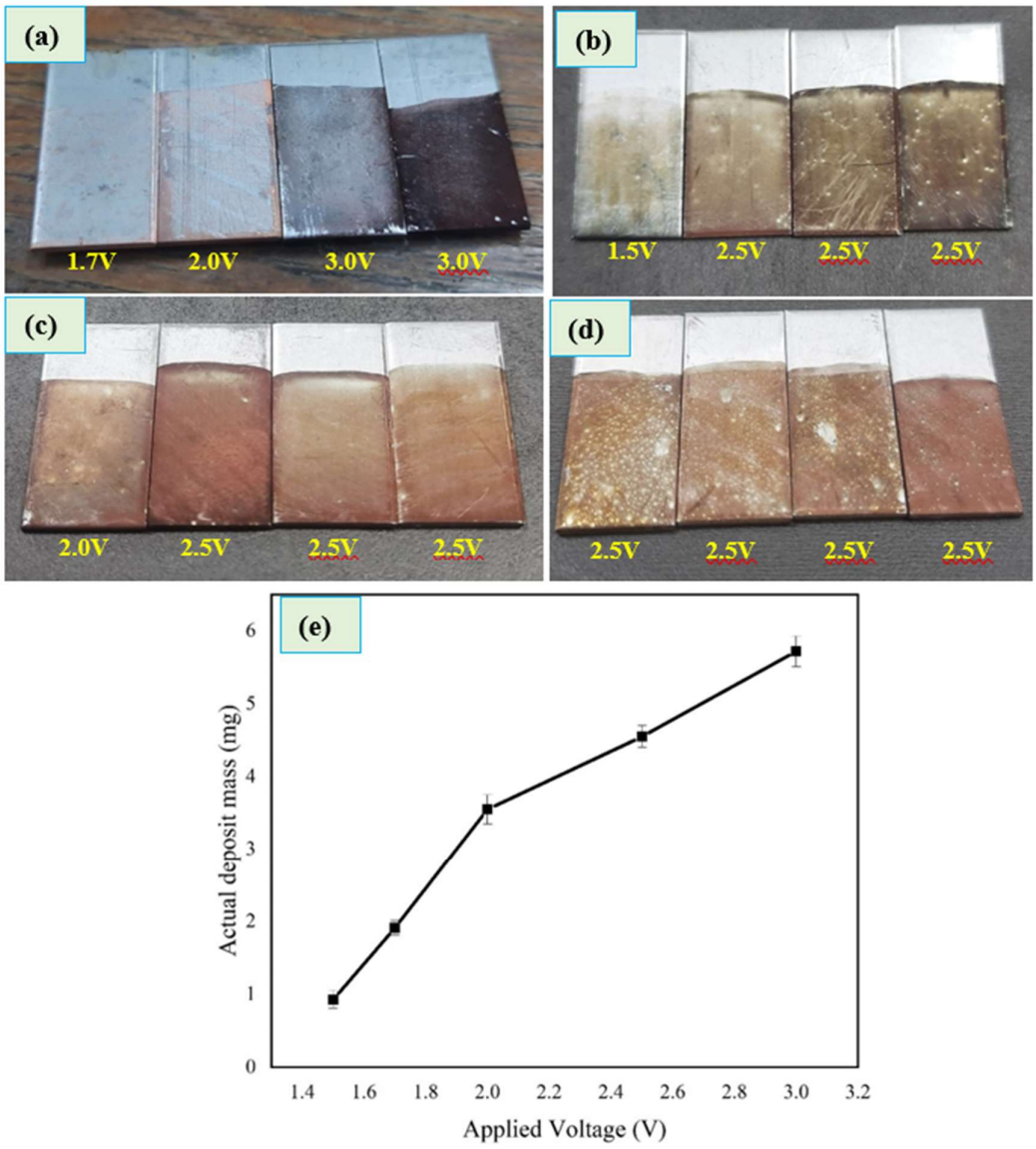

According to Figure 4.7 (d), copper recovery faced some bubble issues, and this happens due to the solution consists of lots of oxygen. Earlier we used the direct solution, where we did not face any bubble forming issues. But using CDI desorption solution, we faced oxygen formation issues. Due to the bubble, the substrates also did not get proper deposition. To get rid of the bubble formation issues, the solution was kept in the vacuum oven for 10 minutes. According to Figure 4.7 (e) the highest amount of actual copper recovery in metallic form found in the applied voltage range between

2.0V and 3.0V. Based on Figure 4.7 and Table shown in the appendix E, the deposition rate increased with the increment of applied voltage. But at the applied voltage of 3.0V, copper started forming copper oxide (CuO), which was appeared as black color. This is why we chose to use the applied voltage in between 2.0V to 3.0V. for the rest of the copper recovery experiments.

4.2.2.2 Effects of Applied Voltage on Nickel

The nickel recovery was primarily performed with varying voltages between 5.0V and 5.5V. These conditions were obtained from the literature. Here, manually prepared 1000ppm nickel nitrate solution was used to deposit the nickel on stainless steel substrate. Boric acid was added to the solution to enhance the nickel deposition rate. Figure 4.8 represents the nickel deposition samples with boric acid and without boric acid.

Initially we deposited nickel without adding boric acid and the deposition rate was very small, which shown in the Figure 4.8 (a). The deposition area was around 3.41cm^2. Based on the literature regarding this issue, we have found that the nickel recovery rate can be further enhanced by adding 3 grams of boric acid to the per 100 ml solution. Hence, we have added the boric acid to enhance the nickel recovery, which shown in Figure 4.8 (b), it's clear that the deposition rate becomes higher after adding boric acid in the solution. Figure 4.8 (c) shown the actual deposit mass of nickel before and after adding boric acid, where the difference was very higher. The actual deposit mass shown in the Appendix E. Therefore, the nickel recovery was performed in the rest of the experiments by adding boric acid. In addition, we maintained the applied voltage in between 5.0V and 5.5V for nickel recovery.

Figure 4.8

Stainless Steel After Nickel Deposition at 5.0V: a) Without Boric Acid and b) With Boric Acid.

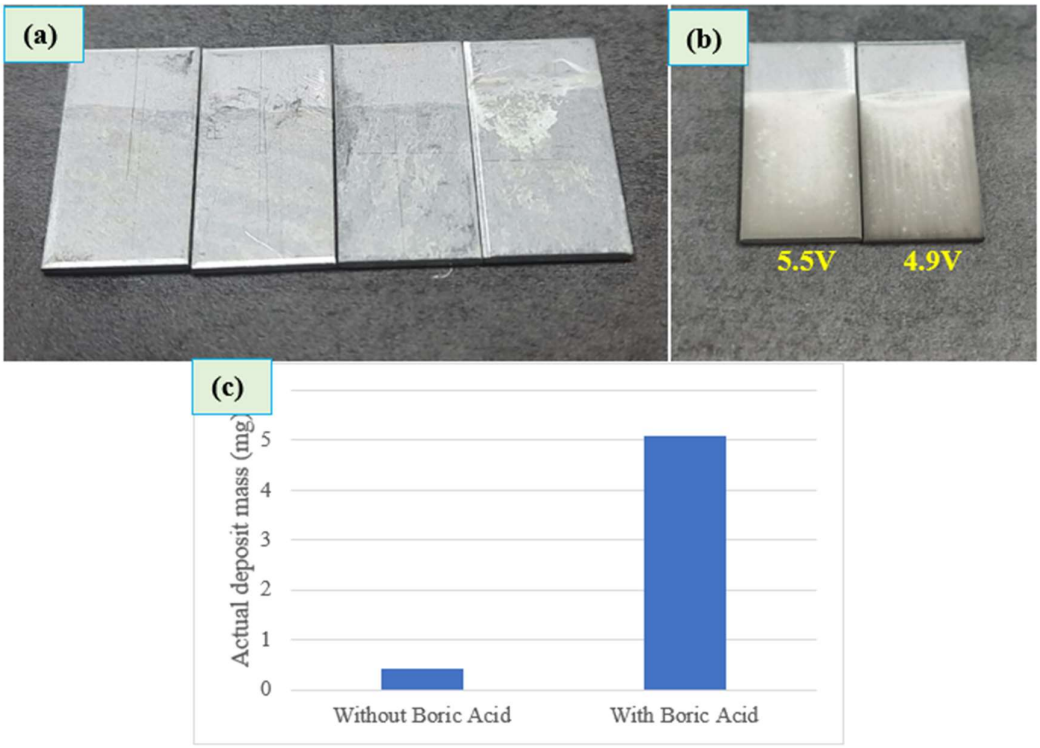

4.2.2.3 Effects of Applied Voltage on Chromium

We have performed the chromium recovery by varying the voltages from 2.0V to 7.0V. For the primary experiment, a manually prepared 1000ppm chromium nitrate solution was used to recover the metallic chromium. Figure 4.9: represents the effect of applied voltage on the chromium recovery.

Figure 4.9 (a) was the first batch of chromium recovery using applied voltage ranges from 2.0V-5.0V. In this experiment, we looked for the appropriate voltage range for chromium recovery. We got the pH range from the Pourbaix diagram. From this experiment, we found no deposition at 2V, and deposition at 3V and 4V was also negligible. But after 4V, we have got some deposition. Hence, by varying the voltages, more samples were deposited, which shown in Figure 4.9 (b). Based on Figure 4.9 (c), the deposition rate was better between 5.0-6.0V. Hence, we continued our further chromium recovery experiments using applied voltage between 5.0V and 6.0V. The actual mass deposition shown in the Appendix E.

Figure 4.9

Stainless Steel After Chromium Deposition Using Different Voltages

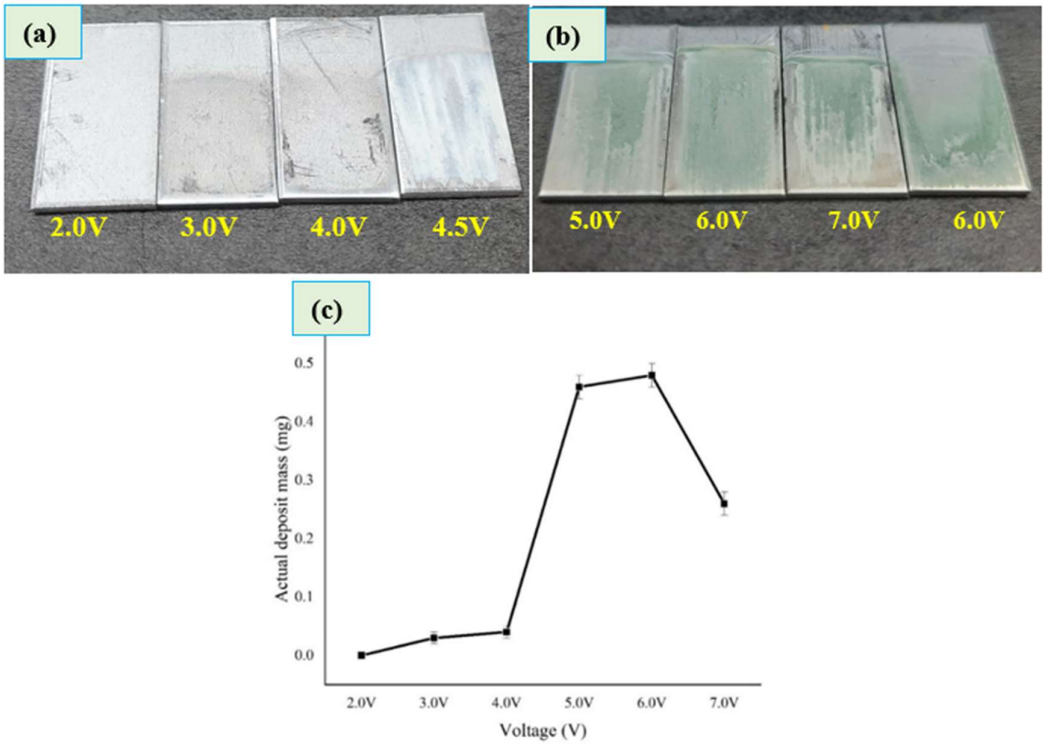

Apart from this, the redox potential plays an important role in the metal recovery. A redox potential is the potential value when the reduction and oxidation of a certain metal or other chemical are in balance with each other. Redox potential is measured in Volt (V). The redox potential of copper (Cu) is +0.337 V. As the copper redox potential is positive hence the copper recovery was more easier than the nickel and chromium recovery. The redox potential of nickel (Ni) is -0.25 V. As the nickel redox potential is negative, therefore the nickel recovery required more energy and difficult to recover in metallic form. The redox potential of chromium (Cr) is -0.74 V. As the chromium redox potential is higher negative, hence the chromium recovery was more difficult to recover in metallic form then copper and nickel.

4.2.3 Effects of pH on Different Metal Species Recovery

In metal recovery, pH plays another most crucial role in recovering the metal. To find out the appropriate pH conditions we performed experiments by varying the different pH value. While we were looking for the appropriate pH value for copper, we kept the

applied voltage fixed around ≈2.5V. we have varied the pH ranges from 1.80 to 5.0. The variation of conditions highlighted and discussed below:

Figure 4.10

Stainless Steel After Copper Deposition at 2.5V by Varying pH.

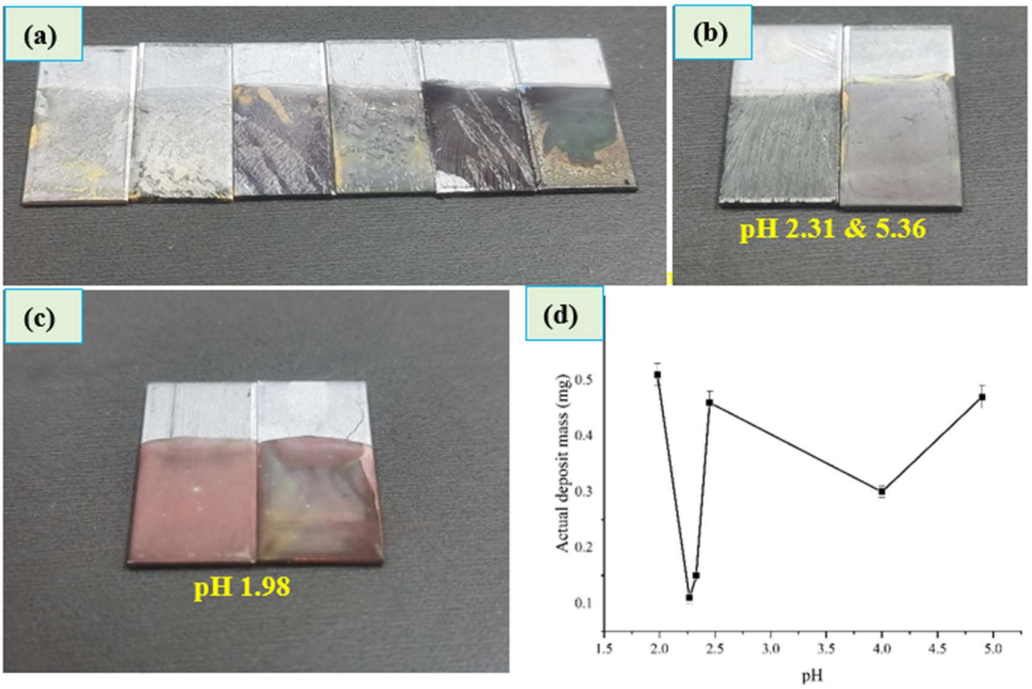

Note: Figure 4.10 (a) and (b) was pH above 2.0. Figure 4.10 (c) pH was less than 2.0.

According to Figure 4.10, here we varied the pH to see the impact on actual copper recovery. During the copper recovery, we have noticed some precipitation, and the color of the deposited copper was different than the genuine metallic copper; this may happen due to the pH was not appropriate, which shown in the Figure 4.10 (a) and (b). The actual metal copper was deposited with a pH below 2.0, shown in Figure 4.10 (c). The actual deposit mass for copper recovery was fluctuating along with the changes of pH. But the actual copper was only obtained with the pH of lower than 2.0. This is why we maintained the pH below 2.0 for the rest of copper recovery experiments.

Primarily, we have performed chromium recovery by adding H_2SO_4 to obtain the chromium deposition. Based on the data analysis, we have found that a pH of around 2.40 to 2.80 was better. We have deposited 20 samples by changing the pH values.

Figure 4.11

Stainless Steel After Chromium Deposition Using 1.5mM Solution at 5.0V: a) pH 3.49, b)2.91, c) 2.66, and d) 2.49.

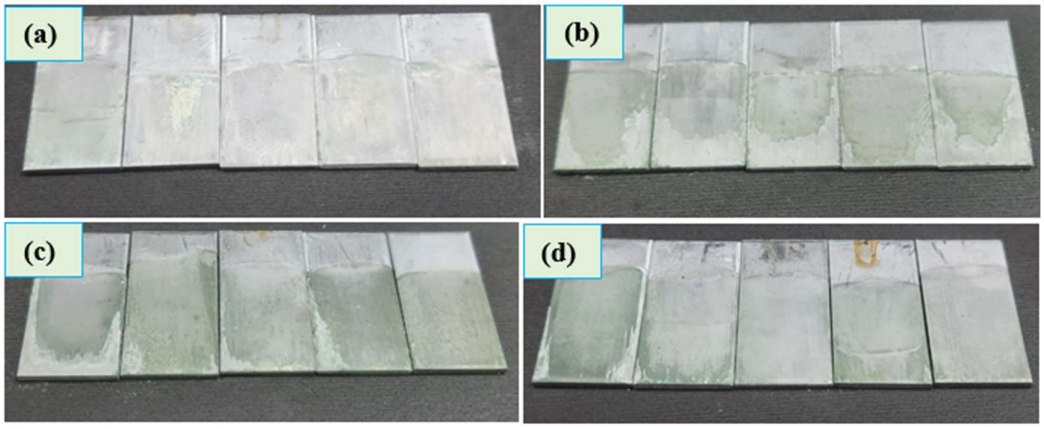

Figure 4.11, we have deposited 4 batch of chromium deposition by varying the pH. Each batch consists of 5 samples. And we have measured the weight 10 times for each sample. Based on the current profile, sample weight, and efficiency analysis, it was observed that the appropriate pH range was around 2.49 and 2.66. Although we were getting good amount of deposition, but the green color deposition was chromium ion not metallic chromium. This is why we deposit more samples using boric acid and different voltage. Figure 4.12 represents the stainless-steel substrate after chromium deposition under varying conditions. we have varied the following conditions:

Sample 1= Chromium Nitrate + 1g Boric Acid at 80ml solution, 5V
Sample 2= Chromium Nitrate + 1g Boric Acid at 80ml solution, 2V
Sample 3= Chromium Nitrate + 2g Boric Acid at 80ml solution, 4V
Sample 4= Chromium Nitrate + 2g Boric Acid at 80ml solution, -5V
Sample 5= Chromium Nitrate + 2g Boric Acid at 80ml solution, 5V
Sample 6= Chromium Nitrate + HCl Acid, 5V

According to Figure 4.12, the actual chromium deposition found using the chromium nitrate with 1 gram of boric acid in per 80 ml solution. Hence, we continued our further chromium recovery experiments using boric acid.

Figure 4.12

Chromium Recovery by Varying Conditions.

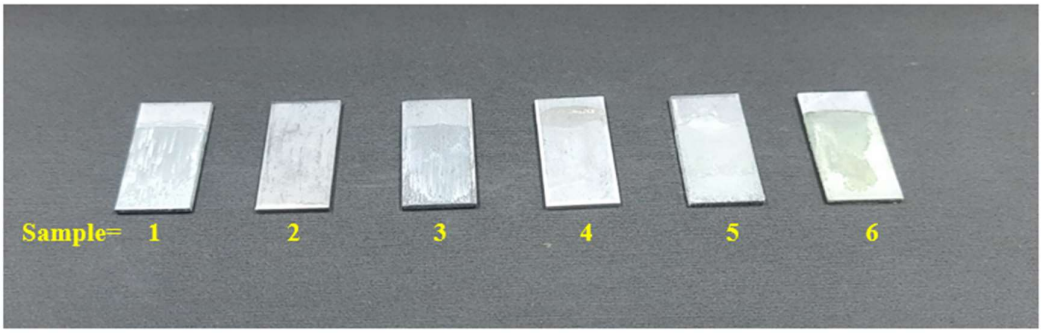

4.2.4 Effect of Concentration on Different Metal Species Recovery

After carefully analyzing the impact of different voltage and pH combinations in section 4.2.2 and 4.2.3, we have found the appropriate range for different metal. The voltage above 2.4V and below 2.8V was better copper deposition without copper oxide formation. In terms of pH, the pH value the lower, the better for copper. Therefore, we have deposited 20 samples by varying concentration to find out the impact of concentration on copper recovery, where voltage around 2.7V and pH around 1.97. Figure 4.13 represents the stainless-steel samples after copper deposition by varying concentration.

Here the Figure 4.13 (a)-(c) shows the actual copper deposition. Appendix F shows the actual deposit mass by varying concentration. According to Figure 4.13 (e), it's clear that the deposition rate increased with the increment of concentration.

Figure 4.13

Stainless Steel After Copper Deposition Using a) 0.5mM, b) 1.5mM, c) 1.6mM, and d) 3.0mM, Copper Nitrate Solution at 2.7V and pH 1.97.

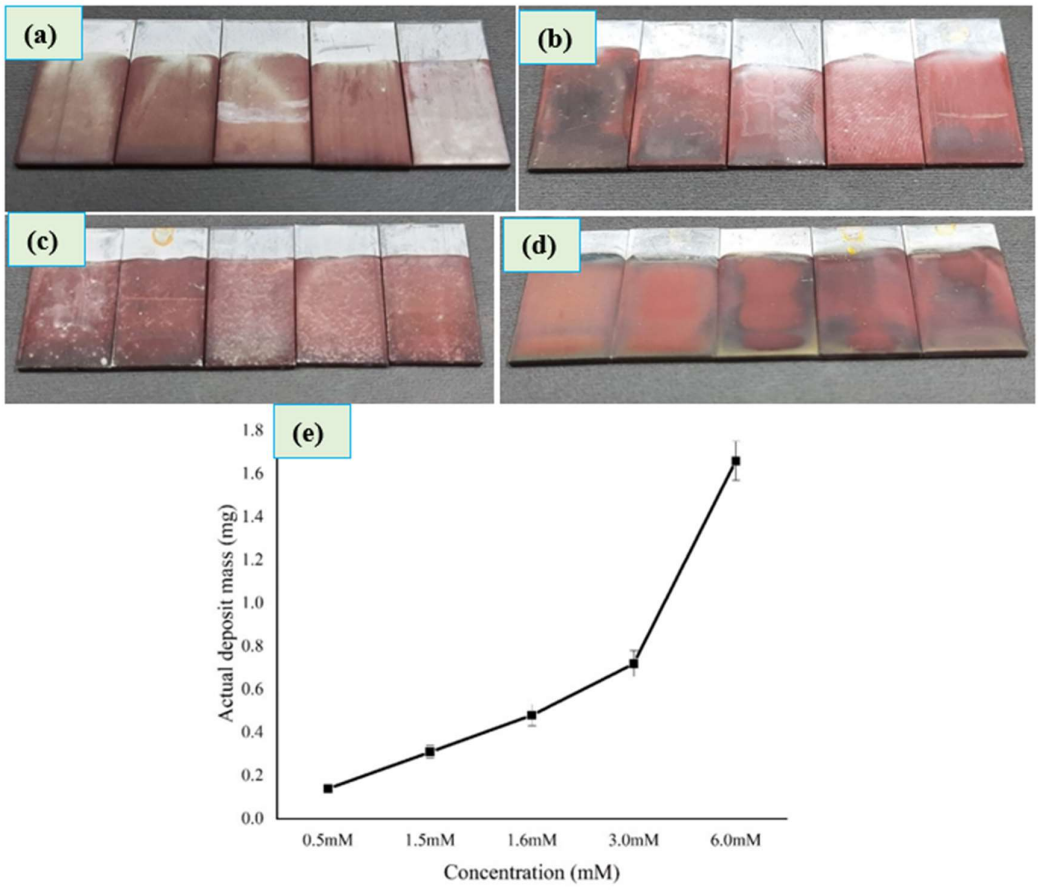

In terms of nickel recovery, based on the section 4.2.2 and 4.2.3 analysis, we have found that the voltage around 5.0-5.5V was appropriate for Nickel recovery. In terms of pH, 3 grams of boric acid were added in the per 100ml solution, whose pH was around 4. We have deposited another 20 samples with varying concentrations, where the applied voltage was around 5V. Figure 4.14 represents the stainless steel after nickel deposition by varying concentration.

Here, we have performed Nickel recovery using different concentrations to find out the deposition trend and recovery efficiency. We have deposited 4 batches of nickel nitrate, shown in Figure 4.14. Each batch consists of 5 samples. Based on the current profile, sample weight, and efficiency analysis, it's clear that the deposition rate was increasing with the increment of concentration.

Figure 4.14

Stainless Steel After Nickel Deposition Using a) 0.5mM, b) 1.5mM, c) 1.6mM, and d) 3.0mM Nickel Nitrate Solution.

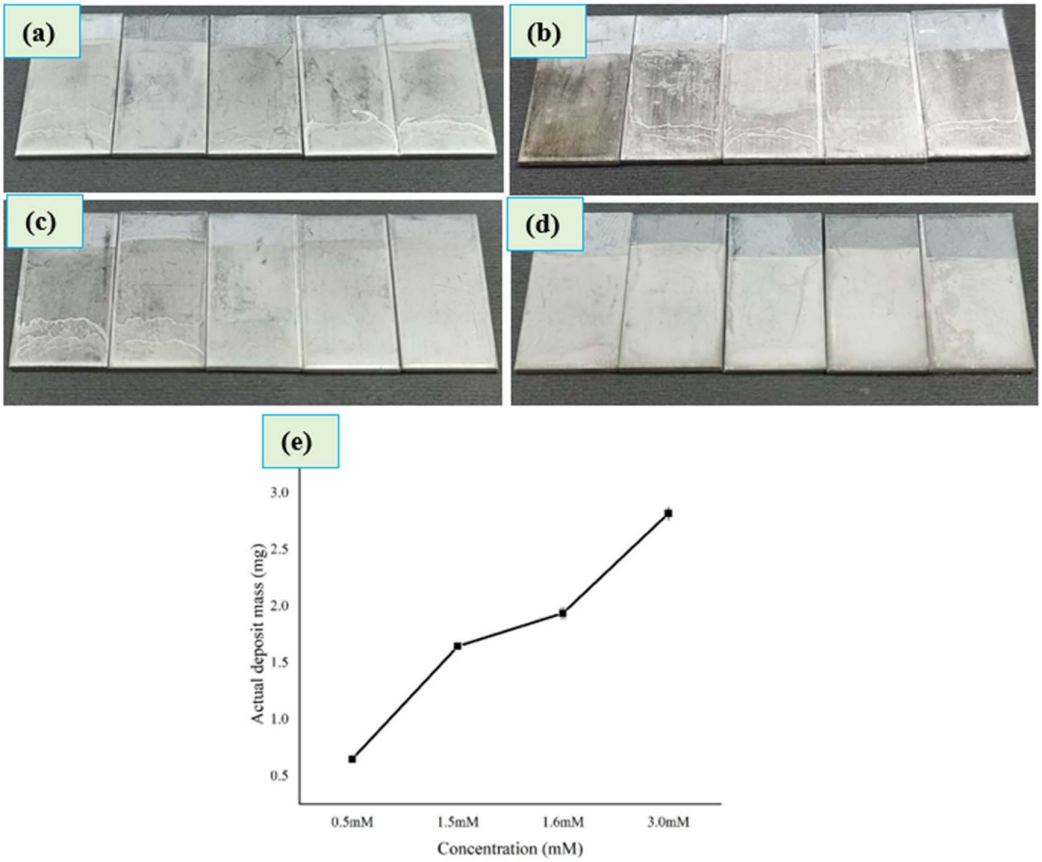

Figure 4.14 (e) also illustrates that the deposition rate was increasing along with the increment of concentration. Without boric acid, the nickel recovery deposition rate was lower, which is shown in Figure 4.8. To adjust the pH, boric acid was added in the solution. Boric acid dramatically increased the metal recovery energy efficiency. The current profile and specific current profile were increasing over time, shown in Appendix B. Because, during the electroplating, the metal is deposited layer by layer. Hence, after some deposition, the steel substrate becomes more resistive, leading to more energy consumption.

In terms chromium recovery, according to the literature and previous experimental analysis from section 4.2.2 and 4.2.3, the deposition of chromium ion using sulfuric acid and hydrochloric acid was not chromium in the metallic form. But by adding the

boric acid, the actual chromium metal was deposited. The appropriate voltage was around 5.0V, and the pH was around 3.0 after adding 3 grams of boric acid in per 80ml of solution. Therefore, 16 samples were deposited by varying the concentration to find out the deposition trend, which shown in Figure 4.15.

Figure 4.15

Stainless Steel After Chromium Deposition Using a) 0.5mM, b) 1.5mM, c) 1.6mM, and d) 3.0mM Chromium Nitrate Solution at 5.0V and pH 4.05.

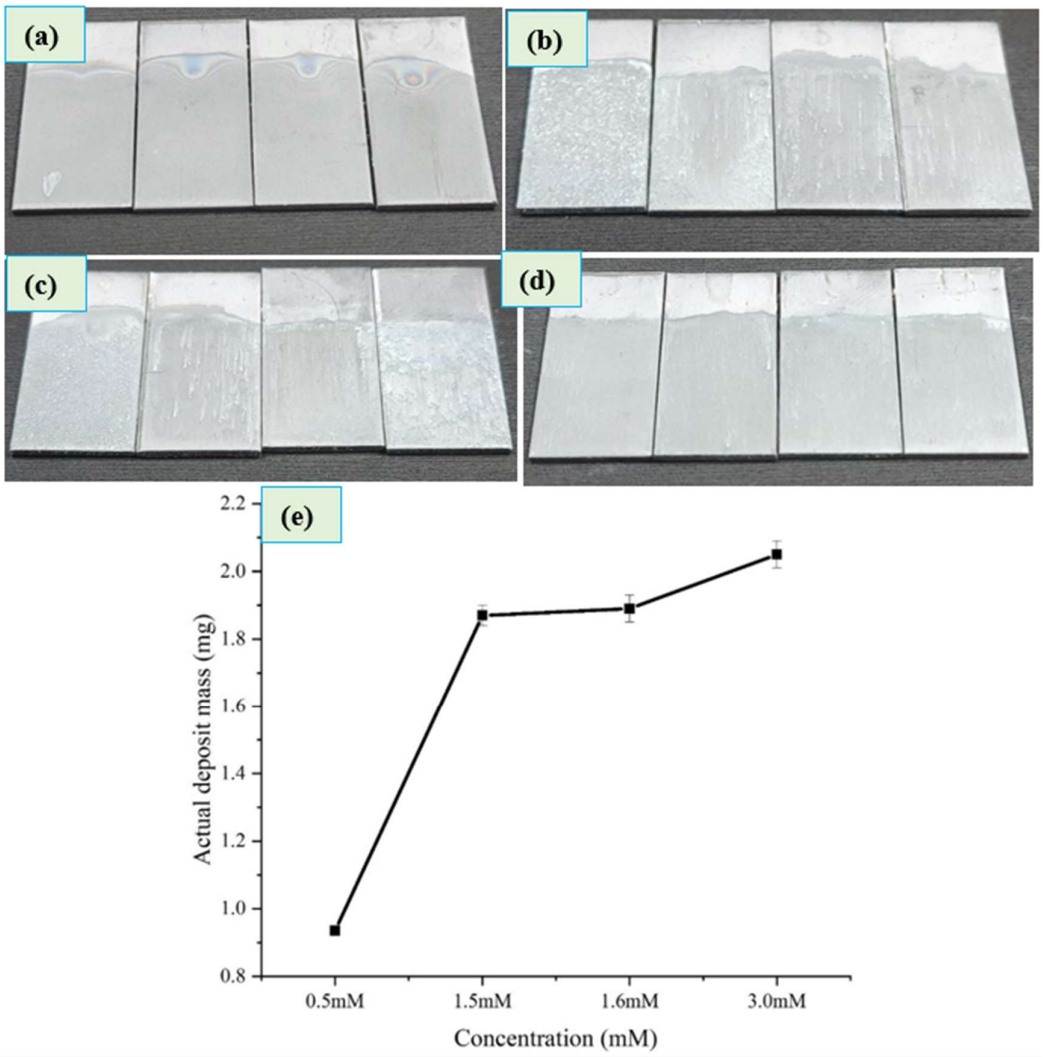

Here, the deposition rate was higher because some boric acid may deposited on the substrate, which appeared as a white dot, shown in Figure 4.15 (b) and (c). Figure 4.15 shows that the deposition ratio was increasing with the increment of concentration.

4.2.5 Characterization of Selected Sample Using AAS

Atomic absorption spectroscopy (AAS) is broadly used to measure the concentration of different metals more accurately. After analyzing the data using mass measurements and faradays law of electrochemistry, few samples have been tested by AAS to see the real deposition ratio. Figures 4.16 were freshly deposited with the copper nitrate solution to get the sample for the AAS test. Appendix B represents the example current profile of the samples.

Figure 4.16

Stainless Steel After Copper Deposition With a) 0.5mM and b) 1.5mM Solution and 2.7V

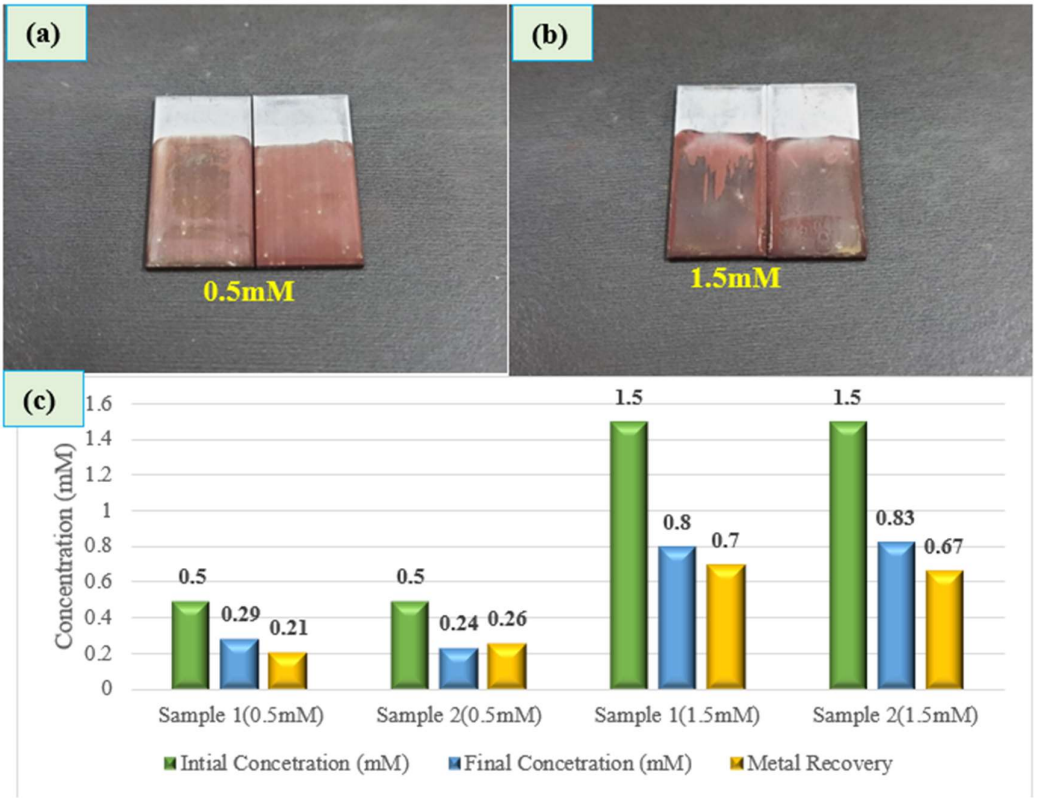

Appendix A represents the calibration curve for copper using the AAS, where the Cu was observed at 324.8nm. The correlation coefficient value was 0.9971. Figure 4.16 (c): represents the actual copper recovery comparison between the initial solution and final solution using AAS data. Appendix G: represent the summary of copper recovery and efficiency data by varying the concentration between 0.5mM and 1.5mM. At 0.5mM, both sample shows 42% and 52% copper recovery efficiency after 1 hour of

deposition, respectively. At 1.5mM concentration, the copper recovery efficiency was 46.6% and 44.6%, respectively. Here the actual metal recovery efficiency was decreased along with the increment of concentration. As the concentration was increasing, but the other parameters like the size of the stainless steel and applied voltage were fixed. As the metal was deposited layer by layer, therefore, the stainless steel becomes more resistive, which leads to less deposition after a certain amount of deposition. Oppositely, lower concentration leads to higher efficiency.

Figures 4.17 were freshly deposited samples with the chromium nitrate solution to get the fresh sample solution for the AAS test.

Figure 4.17

Stainless Steel After Chromium Deposition With a) 0.5mM and b) 1.5mM Solution and 4.9V

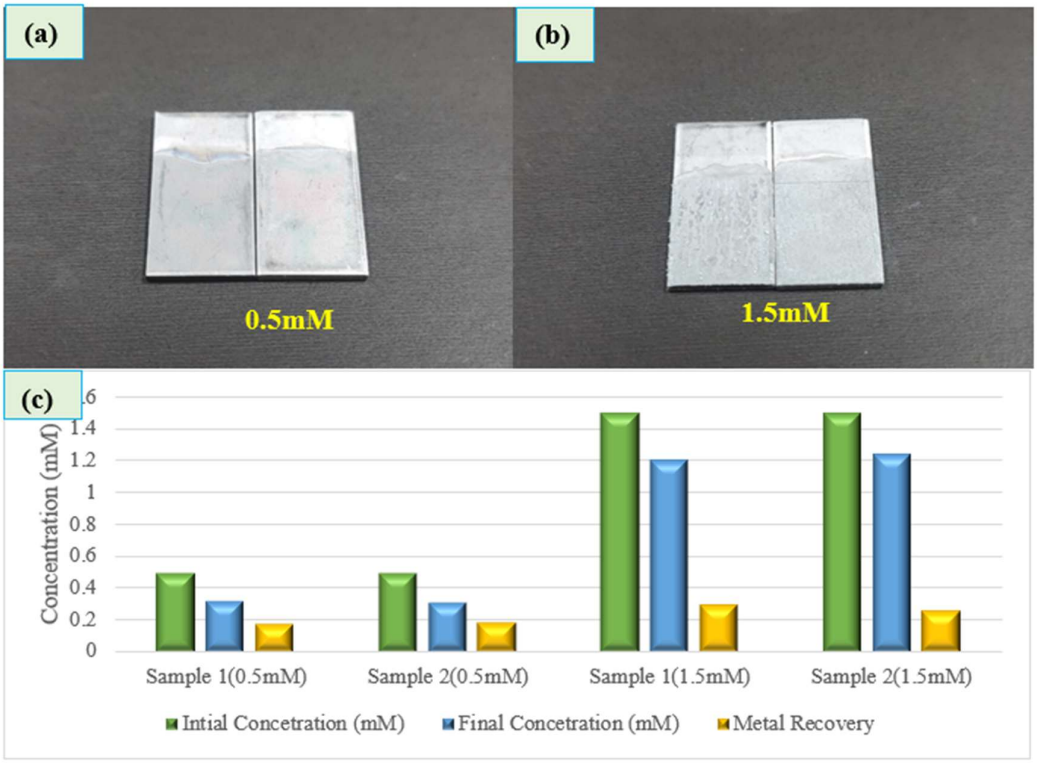

Appendix A represents the calibration curve for chromium using the AAS, where the Cr was observed at 357.9nm. The correlation coefficient value was 0.9977. Using this calibration curve, 4 samples were calculated at 0.5mM and 1.5mM concentrations. Appendix G represents the summary of chromium recovery and efficiency data by

varying the concentration of 0.5mM and 1.5mM. At 0.5mM, both sample shows 34.72% and 37.88% chromium recovery efficiency after 1 hour of deposition, respectively. At 1.5mM concentration, the chromium recovery efficiency was 19.53% and 17.26%, respectively.

4.3 Energy Recovery from CDI cell

This section discusses about the energy recovery from the CDI cell using buck-boost converter and supercapacitor. The energy recovery was performed using copper (Cu^{2+}), Nickel (Ni^{2+}), and Chromium (Cr^{2+}) solution. Figure 3.6 represents the circuit diagram of the energy recovery mechanism.

Figure 4.18 represents the physical energy recovery setup. Buck-boost converter has been used to transfer the energy from the CDI cell to the supercapacitor. As the buck-boost converter rating was not similar to our requirement. Therefore, we were not able to directly transfer the charges from the CDI cell to the supercapacitor. The voltage comparator and operational amplifier have been used to amplify the CDI voltage to a minimum 6 V. Because the buck-boost converter required a minimum of 6V as input, but the CDI output voltage was around 0.1V to 0.3V. Moreover, the capacitance of the CDI cell was around 0.5F, which has been calculated in section 4.1. Hence, the CDI cell was unable to hold the charges for longer period like the supercapacitor with 30 F. Before energy recovery, the CDI adsorption cycle and desorption cycle run for at least 1 cycle to capture the charges. During the adsorption cycle, the flow rate was 5ml/min, so that the CDI could capture more ions. After the adsorption cycle, the energy recovery circuit was connected to the energy recovery circuit to transfer the stored energy to the supercapacitor. When the CDI becomes very close to 0V, the circuit stops working. The detailed methodology described in the Section 3.4. The energy recovery largely depends on the stored energy in the CDI electrodes. The CDI electrode's charges depend on the length of the ion adsorption cycle. Therefore, we have performed energy recovery by varying the cycle duration.

Figure 4.18

Physical Energy Recovery Setup.

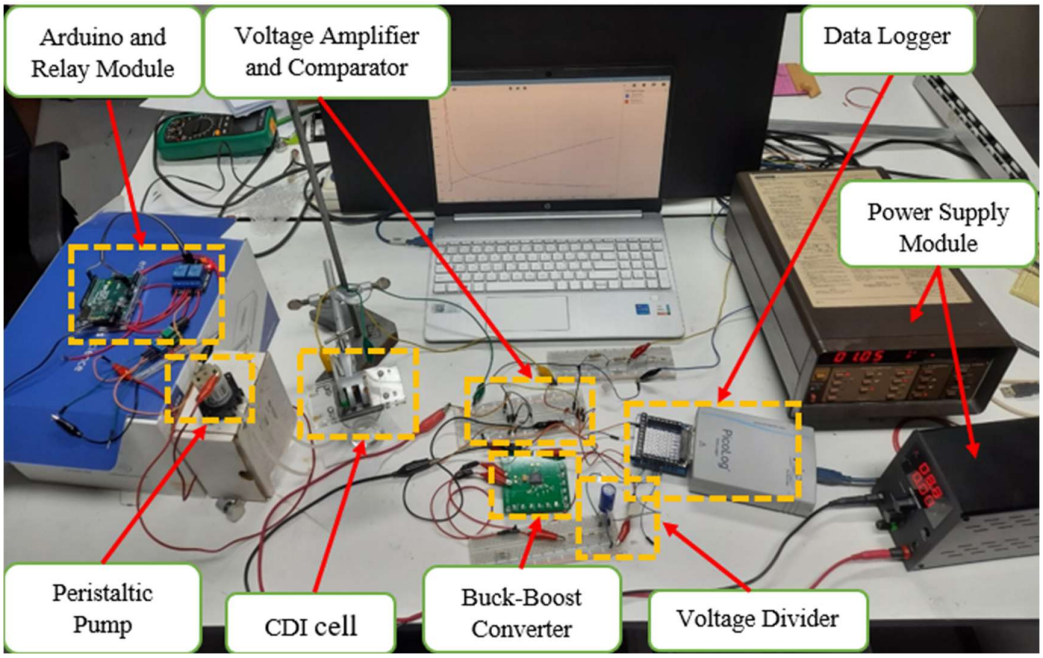

4.3.1 Proof of Concept

After developing the energy recovery circuit, we have performed energy transfer between two supercapacitors to check whether the circuit was working or not. Primarily, we transferred the charges in between two supercapacitors (SC). The circuit was able to transfer charges from one supercapacitor to another. Figure 4.19 represents the SC charging and discharging current vs. time graph, where black line and red line for SC 1 and SC 2 current, respectively. By utilizing which we have calculated the energy transfer efficiency. The equation we used for energy transfer shown in Section 3.4.

Based on Figure 4.19, we were able to transfer the charges from SC 1 to SC 2. The stored energy of SC 1 was 254.93 J. By utilizing our energy recovery circuit, we were able to transfer 175.68J after 1 hour. The energy transfer efficiency was 68.91%. As the circuit was working, therefore we continued energy recovery using this circuit for the rest of the experiments.

Figure 4.19

Charging and Discharging Current vs. Time Graph.

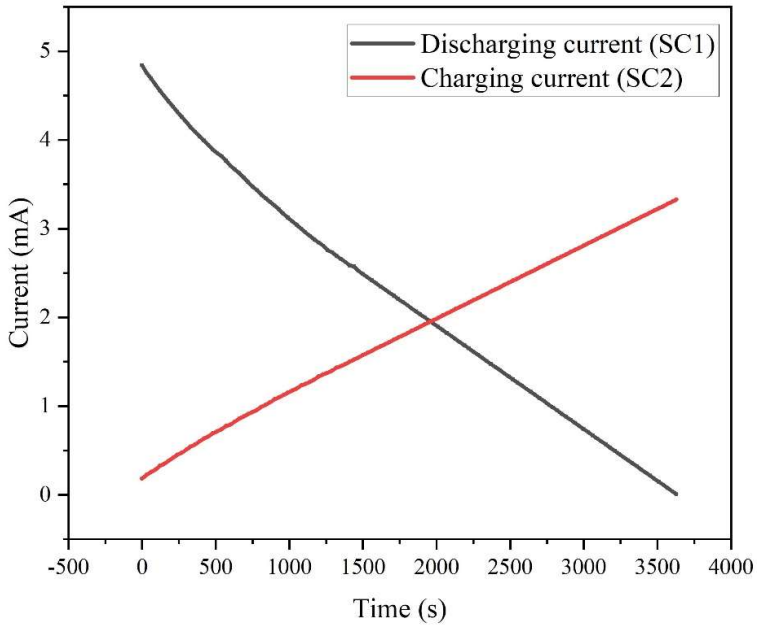

4.3.2 Energy Recovery Using Different Metal Ions

Energy recovery from CDI was performed using different metal ions to find out the energy recovery efficiency. Here we used 1.5mM concentration during the adsorption cycle. The energy recovery largely depends on the number of adsorption cycle duration. We have performed different length of adsorption cycle like 10, 20-, 30-, 40-, and 60-minutes duration. Table 4.2 represents the comparison of stored charges and energy recovery efficiency data based on the cycle duration. Figure 4.20 represents the plot of recovered energy and efficiency over time. The CDI discharging current and SC charging current vs. time profile using copper ion solution, shown in the Appendix H.

Based on Table 4.2, by using the conditions of 10 min cycle, CDI electrodes were able to capture around 53mC. With the 20 min adsorption cycle duration was able to capture around 168mC. The conditions of 30 min and 60 min cycles were able to capture around 267mC and 570mC, respectively. By utilizing the adopted energy recovery mechanism, we were able to transfer energy in between 0.080 J and 0.428J.

Table 4.2

Energy Recovery and Efficiency Comparison Using Cu Ion Solution by Varying Adsorption Cycle Duration.

Ion Ads. Duration (min)	Stored Charges in CDI (mC)	Stored Charges in SC (mC)	Applied Energy (J)	Recovered Energy (J)	Efficiency (%)
10	35.86	3.24	2.59	0.015	0.57
20	168.12	34.67	5.18	0.127	2.44
30	267.86	65.29	7.78	0.242	3.10
40	372.09	103.25	10.37	0.37	3.56
60	570.02	126.80	15.56	0.428	2.74

Figure 4.20

Recovered Energy and Efficiency Plot Over Time Using Copper Ion Solution.

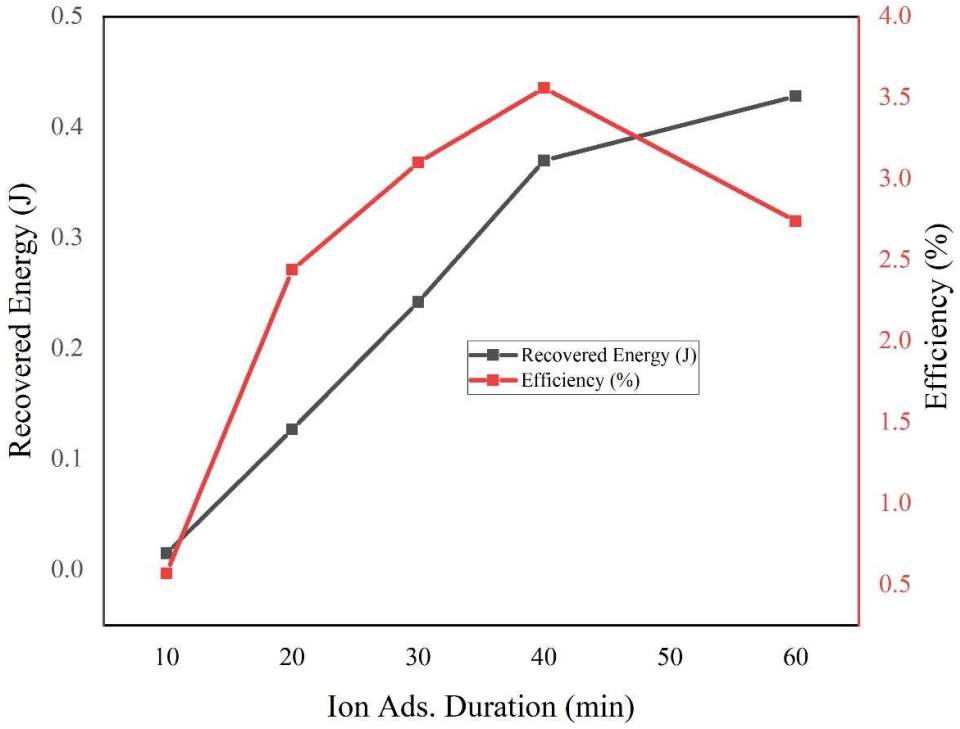

According to Figure 4.20, the energy transfer rate was increasing along with the increment of ion adsorption time. The transfer rate was sharply increasing up to 40 min, then the rate was getting saturated. After 60 min cycle, we did not continue longer cycle

duration because along with the comparison of energy recovery efficiency with the applied energy was not significantly increasing.

In this segment, energy recovery was performed using 1.5mM nickel nitrate solution. Table 4.3 represents the comparison of energy recovery efficiency based on the cycle duration. The CDI discharging current and SC charging current vs. time profile using nickel ion solution, shown in the Appendix H.

Table 4.3

Energy Recovery and Efficiency Comparison Using Ni Ion Solution by Varying Adsorption Cycle Duration.

Ion Ads. Duration (min)	**Stored Charges in CDI (mC)**	**Stored Charges in SC (mC)**	**Applied Energy (J)**	**Recovered Energy (J)**	**Efficiency (%)**
10	12.76	1.59	2.59	0.013	0.50
20	22.27	6.64	5.18	0.092	1.77
30	48.90	13.99	7.78	0.234	3.00
40	322.62	93.01	10.37	0.32	3.08
60	311.87	107.65	15.56	0.356	2.28

Based on Table 4.3, the stored charges in the CDI electrodes were varied by the cycle length. During the 10 min cycle, CDI electrodes were able to capture around 13mC. While with using 60 min cycle duration we were able to capture around 322mC. Using the adopted energy recovery circuit, we were able to transfer the amount of energy in between 0.013 J and 0.356J.

Figure 4.21

Recovered Energy and Efficiency Plot Over Time Using Nickel Ion Solution.

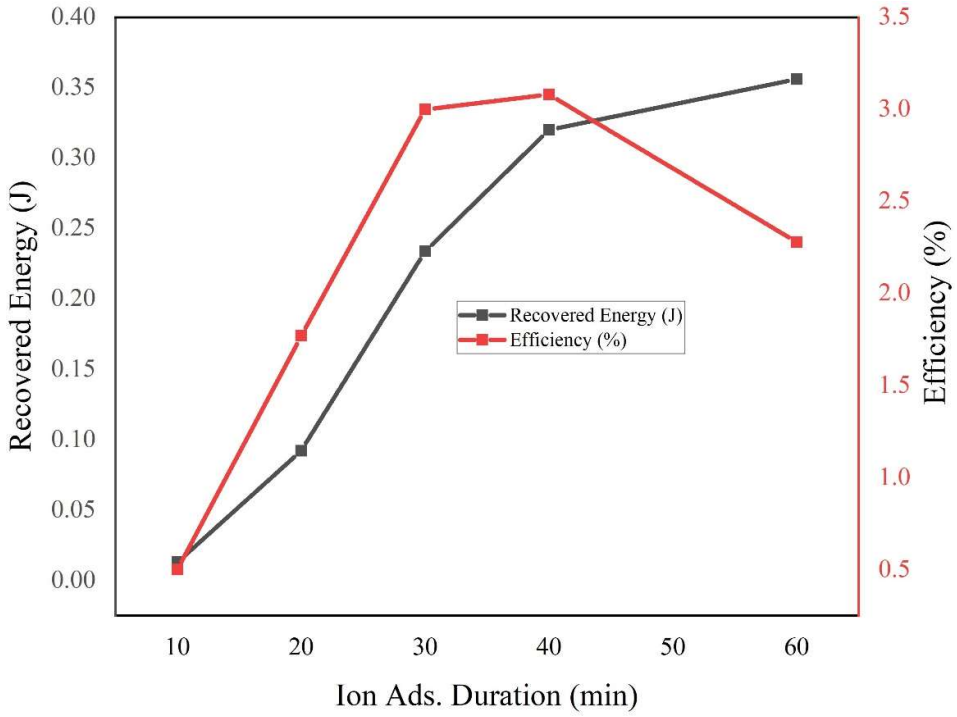

Based on the Figure 4.21, the energy transfer rate was increasing along with the increment of ion adsorption cycle duration. The energy transfer rate was sharply increased up to 40 min cycle, then the energy transfer ratio was getting saturated, and the recovery efficiency was getting lower compared to applied energy.

Table 4.4 represents the comparison of energy recovery efficiency and stored charges based on the cycle duration using chromium ion. The CDI discharging current and SC charging current vs. time profile using chromium, shown in the Appendix H. Figure 4.22 represents the energy recovery vs time graph. Based on Table 4.4, the stored charges in the CDI electrodes were varied by the length of ion adsorption cycle. Using the conditions of 10 min, CDI electrodes were able to capture around 80mC. With the duration of 40 min and 60 min cycles, we were able to capture around 217mC and 482mC, respectively. By utilizing the adopted energy recovery mechanism, we were able to transfer energy in between 0.036 J and 0.370J.

Table 4.4

Energy recovery and efficiency comparison using Cr ion solution by varying adsorption cycle duration.

Ion Ads. Duration (min)	Stored Charges in CDI (mC)	Stored Charges in SC (mC)	Applied Energy (J)	Recovered Energy (J)	Efficiency (%)
10	51.91	9.04	2.59	0.036	1.38
20	50.25	14.32	5.18	0.085	1.63
30	88.99	13.47	7.78	0.152	1.95
40	217.28	42.67	10.37	0.245	2.37
60	482.89	107.98	15.56	0.370	2.36

Figure 4.22

Recovered Energy and Efficiency Plot Over Time Using Chromium Solution.

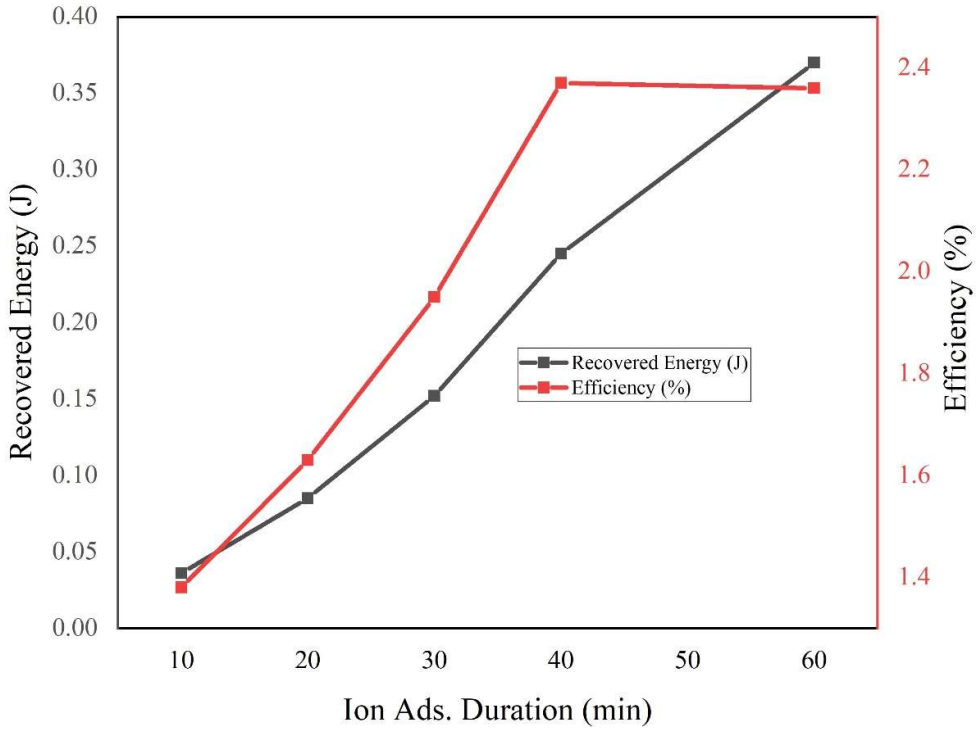

In a nutshell, the amount of transferred energy was increased with the number of cycle and cycle length increments. Figure 4.22, also verify that the energy transfer rate was increasing along with the increment of ion adsorption cycle duration. But the energy recovery efficiency was saturated after 40 min adsorption cycle.

To sum up, the amount of transferred energy and efficiency was increased with the increment of ion adsorption cycle length. Apart from this, atom size of the metal and number of ions also play an important role in the ion absorption, subsequently on energy recovery. Copper has Van der Waals radius of 140 pm, which helps to enter in the electrodes easily compared to nickel and chromium. While nickel and chromium ion have the van der waals radius of 163 pm and 200 pm, respectively. As the copper has lower Van der Waals radius, the energy transfer rate was higher than nickel and chromium. Although chromium has higher radius, but the chromium ion is 3+, hence, Cr ion absorption was higher than nickel, which leads to higher energy transfer rate of chromium than nickel ion. Here the energy recovery efficiency was less than 4%. There can be several reasons behind this lower efficiency. For example, the MnO_2 deposited ACC cloth we used as electrodes in CDI shows almost similar capacitance like plain ACC, which shown in Section 4.2. Therefore, the electrodes were not able holds many charges. It should be also noted that the experiments performed here are using one CDI cell only. By developing a CDI module with multiple cells working together, one can expect to recover more energy from the system and hence overall energy recovery efficiency can be improved further.

CHAPTER 5
CONCLUSION AND FUTURE RECOMMENDATIONS

A MnO_2-ACC CDI cell was constructed to perform metal and energy recovery. Adsorption and desorption current profile analysis was performed using the constructed CDI cell to compare the behavior with the ideal CDI cell. Based on the absorption and desorption current profile analysis, the current behavior was similar to the ideal CDI cell. In terms of metal recovery, appropriate applied voltage ranges were identified for the three types of heavy metal. For copper recovery, the better-applied voltage was 2.4V-2.7V for better deposition. According to the experiment, a pH below 2.0 was better to avoid copper oxide formation. For nickel recovery, the appropriate voltage was around 5.0V-5.5V for higher recovery. For chromium recovery, the appropriate applied voltage was identified as around 5.0V. To enhance the metal recovery, boric acid was utilized for chromium and nickel. According to the AAS test, for copper, the recovery efficiency was 52% and 46.6% for the 0.5mM and 1.5mM, respectively. In terms of chromium, the recovery efficiency was 37.88% and 19.53% for the 0.5mM and 1.5mM, respectively. In terms of energy recovery, the recovered energy efficiency was 3.56%, 3.08%, and 2.37% for copper, nickel, and chromium, respectively. The energy recovery efficiency was increased up to 40 min ion adsorption cycle, and then the efficiency started reducing.

This work can be further extended by developing a buck-boost converter with similar ratings to the CDI cell, which will help in more efficient energy recovery by directly transferring the energy to the SC without the help of a voltage amplifier. Moreover, this work can be extended by using multiple metal ions together. Furthermore, a single cell can be developed to directly recovered the metal without the two separate stages like desorption solution preparation and subsequently metal recovery.

REFERENCES

Ajao, V., Nam, K., Chatzopoulos, P., Spruijt, E., Bruning, H., Rijnaarts, H., & Temmink, H. (2020). Regeneration and reuse of microbial extracellular polymers immobilised on a bed column for heavy metal recovery. *Water Research*, *171*, 115472. https://doi.org/10.1016/J.WATRES.2020.115472

Alkuran, M., Orabi, M., & Seheinberg, N. (2008a). Highly efficient capacitive de-ionization (CDI) water purification system using a buck-boost converter. *Conference Proceedings - IEEE Applied Power Electronics Conference and Exposition - APEC*, 1926–1930. https://doi.org/10.1109/APEC.2008.4522991

Alkuran, M., Orabi, M., & Seheinberg, N. (2008b). Highly efficient capacitive de-ionization (CDI) water purification system using a buck-boost converter. *Conference Proceedings - IEEE Applied Power Electronics Conference and Exposition - APEC*, 1926–1930. https://doi.org/10.1109/APEC.2008.4522991

Almomani, F., Bhosale, R., Khraisheh, M., kumar, A., & Almomani, T. (2020). Heavy metal ions removal from industrial wastewater using magnetic nanoparticles (MNP). *Applied Surface Science*, *506*, 144924. https://doi.org/10.1016/J.APSUSC.2019.144924

Aneke, M., & Wang, M. (2016). Energy storage technologies and real life applications – A state of the art review. *Applied Energy*, *179*, 350–377. https://doi.org/10.1016/J.APENERGY.2016.06.097

Armstrong, R. D., Todd, M., Atkinson, J. W., & Scott, K. (1996). Selective electrodeposition of metals from simulated waste solutions. *Journal of Applied Electrochemistry 1996 26:4*, *26*(4), 379–384. https://doi.org/10.1007/BF00251322

Biesheuvel, P. M., & van der Wal, A. (2010). Membrane capacitive deionization. *Journal of Membrane Science*, *346*(2), 256–262. https://doi.org/10.1016/J.MEMSCI.2009.09.043

Carvalho Barros, G. K. G., Melo, R. P. F., & Barros Neto, E. L. de. (2018). Removal of copper ions using sodium hexadecanoate by ionic flocculation. *Separation and Purification Technology*, *200*, 294–299. https://doi.org/10.1016/J.SEPPUR.2018.01.062

Chang, Z., Li, F., Qi, X., Jiang, B., Kou, J., & Sun, C. (2020). Selective and efficient adsorption of Au (III) in aqueous solution by Zr-based metal-organic frameworks (MOFs): An unconventional way for gold recycling. *Journal of Hazardous Materials*, *391*, 122175. https://doi.org/10.1016/J.JHAZMAT.2020.122175

Changchien, S. K., Liang, T. J., Chen, J. F., & Yang, L. S. (2010). Novel high step-up DCDC converter for fuel cell energy conversion system. *IEEE Transactions on*

Industrial Electronics, *57*(6), 2007–2017. https://doi.org/10.1109/TIE.2009.2026364

Chen, L., Yin, X., Zhu, L., & Qiu, Y. (2018). Energy recovery and electrode regeneration under different charge/discharge conditions in membrane capacitive deionization. *Desalination*, *439*, 93–101. https://doi.org/10.1016/J.DESAL.2018.04.012

Chen, T.-C., Priambodo, R., Huang, R.-L., & Huang, Y.-H. (2013). The Effective Electrolytic Recovery of Dilute Copper from Industrial Wastewater. *Journal of Waste Management*, *2013*, 1–6. https://doi.org/10.1155/2013/164780

Chen, Y. W., Chen, J. F., Lin, C. H., & Hou, C. H. (2019). Integrating a supercapacitor with capacitive deionization for direct energy recovery from the desalination of brackish water. *Applied Energy*, *252*, 113417. https://doi.org/10.1016/J.APENERGY.2019.113417

Chen, Z., Zhang, H., Wu, C., Wang, Y., & Li, W. (2015). A study of electrosorption selectivity of anions by activated carbon electrodes in capacitive deionization. *Desalination*, *369*, 46–50. https://doi.org/10.1016/J.DESAL.2015.04.022

Dehkhoda, A. M., Ellis, N., & Gyenge, E. (2016). Effect of activated biochar porous structure on the capacitive deionization of NaCl and ZnCl2 solutions. *Microporous and Mesoporous Materials*, *224*, 217–228. https://doi.org/10.1016/J.MICROMESO.2015.11.041

Demirbas, A. (2008). Heavy metal adsorption onto agro-based waste materials: A review. *Journal of Hazardous Materials*, *157*(2–3), 220–229. https://doi.org/10.1016/J.JHAZMAT.2008.01.024

DeNooyer, T. A., Peschel, J. M., Zhang, Z., & Stillwell, A. S. (2016). Integrating water resources and power generation: The energy–water nexus in Illinois. *Applied Energy*, *162*, 363–371. https://doi.org/10.1016/J.APENERGY.2015.10.071

Długołęcki, P., & Wal, A. van der. (2013). Energy Recovery in Membrane Capacitive Deionization. *Environmental Science and Technology*, *47*(9), 4904–4910. https://doi.org/10.1021/ES3053202

Dondi, D., Bertacchini, A., Brunelli, D., Larcher, L., & Benini, L. (2008). Modeling and optimization of a solar energy harvester system for self-powered wireless sensor networks. *IEEE Transactions on Industrial Electronics*, *55*(7), 2759–2766. https://doi.org/10.1109/TIE.2008.924449

Dykstra, J. E., Porada, S., van der Wal, A., & Biesheuvel, P. M. (2018). Energy consumption in capacitive deionization – Constant current versus constant voltage operation. *Water Research*, *143*, 367–375. https://doi.org/10.1016/J.WATRES.2018.06.034

Fang, D., & Chen, B. (2017). Linkage analysis for the water–energy nexus of city. *Applied Energy*, *189*, 770–779. https://doi.org/10.1016/J.APENERGY.2016.04.020

García-Quismondo, E., Santos, C., Lado, J., Palma, J., & Anderson, Marc. A. (2013). Optimizing the Energy Efficiency of Capacitive Deionization Reactors Working under Real-World Conditions. *Environmental Science and Technology*, *47*(20), 11866–11872. https://doi.org/10.1021/ES4021603

González, A., Goikolea, E., Barrena, J. A., & Mysyk, R. (2016). Review on supercapacitors: Technologies and materials. *Renewable and Sustainable Energy Reviews*, *58*, 1189–1206. https://doi.org/10.1016/J.RSER.2015.12.249

Griggs, D., Stafford-Smith, M., Gaffney, O., Rockström, J., Öhman, M. C., Shyamsundar, P., Steffen, W., Glaser, G., Kanie, N., & Noble, I. (2013). Sustainable development goals for people and planet. *Nature 2013 495:7441*, *495*(7441), 305–307. https://doi.org/10.1038/495305a

Huang, C. C., & Su, Y. J. (2010). Removal of copper ions from wastewater by adsorption/electrosorption on modified activated carbon cloths. *Journal of Hazardous Materials*, *175*(1–3), 477–483. https://doi.org/10.1016/J.JHAZMAT.2009.10.030

Jande, Y. A. C., & Kim, W. S. (2013). Desalination using capacitive deionization at constant current. *Desalination*, *329*, 29–34. https://doi.org/10.1016/J.DESAL.2013.08.023

Jeon, S., Yeo, J., Yang, S., Choi, J., & Kim, D. K. (2014a). Ion storage and energy recovery of a flow-electrode capacitive deionization process. *Journal of Materials Chemistry A*, *2*(18), 6378–6383. https://doi.org/10.1039/C4TA00377B

Jeon, S., Yeo, J., Yang, S., Choi, J., & Kim, D. K. (2014b). Ion storage and energy recovery of a flow-electrode capacitive deionization process. *Journal of Materials Chemistry A*, *2*(18), 6378–6383. https://doi.org/10.1039/C4TA00377B

Kang, J., Kim, T., Jo, K., & Yoon, J. (2014). Comparison of salt adsorption capacity and energy consumption between constant current and constant voltage operation in capacitive deionization. *Desalination*, *352*, 52–57. https://doi.org/10.1016/J.DESAL.2014.08.009

Kang, J., Kim, T., Shin, H., Lee, J., Ha, J. I., & Yoon, J. (2016a). Direct energy recovery system for membrane capacitive deionization. *Desalination*, *398*, 144–150. https://doi.org/10.1016/J.DESAL.2016.07.025

Kang, J., Kim, T., Shin, H., Lee, J., Ha, J. I., & Yoon, J. (2016b). Direct energy recovery system for membrane capacitive deionization. *Desalination*, *398*, 144–150. https://doi.org/10.1016/J.DESAL.2016.07.025

Kim, D. I., Gwak, G., Dorji, P., He, D., Phuntsho, S., Hong, S., & Shon, H. (2017). Palladium Recovery through Membrane Capacitive Deionization from Metal Plating Wastewater. *ACS Sustainable Chemistry and Engineering*, *6*(2), 1692–1701. https://doi.org/10.1021/ACSSUSCHEMENG.7B02923

Kobayashi, K., Matsuo, H., & Sekine, Y. (2006). Novel solar-cell power supply system using a multiple-input DC - DC converter. *IEEE Transactions on Industrial Electronics*, *53*(1), 281–286. https://doi.org/10.1109/TIE.2005.862250

Li, H., & Zou, L. (2011). Ion-exchange membrane capacitive deionization: A new strategy for brackish water desalination. *Desalination*, *275*(1–3), 62–66. https://doi.org/10.1016/J.DESAL.2011.02.027

Li, P. P., Peng, C. S., Li, F. M., Song, S. X., & Juan, A. O. (2011). Copper and Nickel Recovery from Electroplating Sludge by the Process of Acid-leaching and Electro-depositing. *International Journal of Environmental Research*, *5*(3), 797–804. https://doi.org/10.22059/IJER.2011.386

Liu, C., Wu, T., Hsu, P.-C., Xie, J., Zhao, J., Liu, K., Sun, J., Xu, J., Tang, J., Ye, Z., Lin, D., & Cui, Y. (2019). Direct/Alternating Current Electrochemical Method for Removing and Recovering Heavy Metal from Water Using Graphene Oxide Electrode. *ACS Nano*, *13*(6), 6431–6437. https://doi.org/10.1021/ACSNANO.8B09301

Liu, P., Yan, T., Zhang, J., Shi, L., & Zhang, D. (2017). Separation and recovery of heavy metal ions and salt ions from wastewater by 3D graphene-based asymmetric electrodes via capacitive deionization. *Journal of Materials Chemistry A*, *5*(28), 14748–14757. https://doi.org/10.1039/C7TA03515B

Luo, X., Wang, J., Dooner, M., & Clarke, J. (2015). Overview of current development in electrical energy storage technologies and the application potential in power system operation. *Applied Energy*, *137*, 511–536. https://doi.org/10.1016/J.APENERGY.2014.09.081

Ma, J., Liang, P., Sun, X., Zhang, H., Bian, Y., Yang, F., Bai, J., Gong, Q., & Huang, X. (2019). Energy recovery from the flow-electrode capacitive deionization. *Journal of Power Sources*, *421*, 50–55. https://doi.org/10.1016/J.JPOWSOUR.2019.02.082

Min, K. J., Choi, S. Y., Jang, D., Lee, J., & Park, K. Y. (2019). Separation of metals from electroplating wastewater using electrodialysis. *Https://Doi.Org/10.1080/15567036.2019.1568629*, *41*(20), 2471–2480. https://doi.org/10.1080/15567036.2019.1568629

Nepel, T. C. de M., Costa, J. M., Gurgel Adeodato Vieira, M., & Almeida Neto, A. F. de. (2020). Copper removal kinetic from electroplating industry wastewater using pulsed electrodeposition technique. *Https://Doi.Org/10.1080/09593330.2020.1793005*, 1–22. https://doi.org/10.1080/09593330.2020.1793005

Nymand, M., & Andersen, M. A. E. (2010). High-efficiency isolated boost DCDC converter for high-power low-voltage fuel-cell applications. *IEEE Transactions on Industrial Electronics*, *57*(2), 505–514. https://doi.org/10.1109/TIE.2009.2036024

Omosebi, A., Li, Z., Holubowitch, N., Gao, X., Landon, J., Cramer, A., & Liu, K. (2020). Energy recovery in capacitive deionization systems with inverted operation characteristics. *Environmental Science: Water Research & Technology*, *6*(2), 321–330. https://doi.org/10.1039/C9EW00797K

Oyarzun, D. I., Hawks, S. A., Campbell, P. G., Hemmatifar, A., Krishna, A., Santiago, J. G., & Stadermann, M. (2020). Energy transfer for storage or recovery in capacitive deionization using a DC-DC converter. *Journal of Power Sources*, *448*, 227409. https://doi.org/10.1016/J.JPOWSOUR.2019.227409

Peng, C., Liu, Y., Bi, J., Xu, H., & Ahmed, A. S. (2011). Recovery of copper and water from copper-electroplating wastewater by the combination process of electrolysis and electrodialysis. *Journal of Hazardous Materials*, *189*(3), 814–820. https://doi.org/10.1016/J.JHAZMAT.2011.03.034

Pernia, A. M., Alvarez-Gonzalez, F. J., Prieto, M. A. J., Villegas, P. J., & Nuno, F. (2014). New control strategy of an up-down converter for energy recovery in a CDI desalination system. *IEEE Transactions on Power Electronics*, *29*(7), 3573–3581. https://doi.org/10.1109/TPEL.2013.2280814

Pernía, A. M., Norniella, J. G., Martín-Ramos, J. A., Díaz, J., & Martínez, J. A. (2012). Up-down converter for energy recovery in a CDI desalination system. *IEEE Transactions on Power Electronics*, *27*(7), 3257–3265. https://doi.org/10.1109/TPEL.2011.2180926

Porada, S., Zhao, R., van der Wal, A., Presser, V., & Biesheuvel, P. M. (2013). Review on the science and technology of water desalination by capacitive deionization. *Progress in Materials Science*, *58*(8), 1388–1442. https://doi.org/10.1016/J.PMATSCI.2013.03.005

Porada, S., Zhao, R., Van Der Wal, A., Presser, V., & Biesheuvel, P. M. (2013). Review on the science and technology of water desalination by capacitive deionization. In *Progress in Materials Science* (Vol. 58, Issue 8, pp. 1388–1442). Elsevier Ltd. https://doi.org/10.1016/j.pmatsci.2013.03.005

Qasem, N. A. A., Mohammed, R. H., & Lawal, D. U. (2021). Removal of heavy metal ions from wastewater: a comprehensive and critical review. *Npj Clean Water 2021 4:1*, *4*(1), 1–15. https://doi.org/10.1038/s41545-021-00127-0

Qu, Y., Campbell, P. G., Gu, L., Knipe, J. M., Dzenitis, E., Santiago, J. G., & Stadermann, M. (2016). Energy consumption analysis of constant voltage and constant current operations in capacitive deionization. *Desalination*, *400*, 18–24. https://doi.org/10.1016/J.DESAL.2016.09.014

Ramachandran, A., Hawks, S. A., Stadermann, M., & Santiago, J. G. (2018). Frequency analysis and resonant operation for efficient capacitive deionization. *Water Research*, *144*, 581–591. https://doi.org/10.1016/J.WATRES.2018.07.066

Ritchie, S. M. C., & Bhattacharyya, D. (2002). Membrane-based hybrid processes for high water recovery and selective inorganic pollutant separation. *Journal of*

Hazardous Materials, *92*(1), 21–32. https://doi.org/10.1016/S0304-3894(01)00370-3

Rommerskirchen, A., Linnartz, C. J., Müller, D., Willenberg, L. K., & Wessling, M. (2018). Energy Recovery and Process Design in Continuous Flow–Electrode Capacitive Deionization Processes. *ACS Sustainable Chemistry & Engineering*, *6*(10), 13007–13015. https://doi.org/10.1021/ACSSUSCHEMENG.8B02466

Shang, Y., Hei, P., Lu, S., Shang, L., Li, X., Wei, Y., Jia, D., Jiang, D., Ye, Y., Gong, J., Lei, X., Hao, M., Qiu, Y., Liu, J., & Wang, H. (2018). China's energy-water nexus: Assessing water conservation synergies of the total coal consumption cap strategy until 2050. *Applied Energy*, *210*, 643–660. https://doi.org/10.1016/J.APENERGY.2016.11.008

Tan, C., He, C., Fletcher, J., & Waite, T. D. (2020). Energy recovery in pilot scale membrane CDI treatment of brackish waters. *Water Research*, *168*, 115146. https://doi.org/10.1016/J.WATRES.2019.115146

Vakili, M., Deng, S., Cagnetta, G., Wang, W., Meng, P., Liu, D., & Yu, G. (2019). Regeneration of chitosan-based adsorbents used in heavy metal adsorption: A review. *Separation and Purification Technology*, *224*, 373–387. https://doi.org/10.1016/J.SEPPUR.2019.05.040

Vardhan, K. H., Kumar, P. S., & Panda, R. C. (2019). A review on heavy metal pollution, toxicity and remedial measures: Current trends and future perspectives. *Journal of Molecular Liquids*, *290*, 111197. https://doi.org/10.1016/J.MOLLIQ.2019.111197

Wang, C., Chen, L., & Liu, S. (2019). Activated carbon fiber for adsorption/electrodeposition of Cu (II) and the recovery of Cu (0) by controlling the applied voltage during membrane capacitive deionization. *Journal of Colloid and Interface Science*, *548*, 160–169. https://doi.org/10.1016/J.JCIS.2019.04.030

Wang, G., Zhang, L., & Zhang, J. (2012). A review of electrode materials for electrochemical supercapacitors. *Chemical Society Reviews*, *41*(2), 797–828. https://doi.org/10.1039/C1CS15060J

Wang, Z., Yue, L., Liu, Z.-T., Liu, Z.-H., & Hao, Z. (2012). Functional graphene nanocomposite as an electrode for the capacitive removal of FeCl3 from water. *Journal of Materials Chemistry*, *22*(28), 14101–14107. https://doi.org/10.1039/C2JM32175K

Win, K. K., Dasgupta, S., & Panda, S. K. (2011). An optimized MPPT circuit for thermoelectric energy harvester for low power applications. *8th International Conference on Power Electronics - ECCE Asia: "Green World with Power Electronics", ICPE 2011-ECCE Asia*, 1579–1584. https://doi.org/10.1109/ICPE.2011.5944535

Zhan, Y., Nie, C., Pan, L., Li, H., & Sun, Z. (2011). Electrical Removal Behavior of Carbon Nanotube and Carbon Nanofiber Film in CuCl 2 Solution: Kinetics and

Thermodynamics Study . *International Journal of Electrochemistry*, *2011*, 1–8. https://doi.org/10.4061/2011/572862

Zhao, F., Peydayesh, M., Ying, Y., Mezzenga, R., & Ping, J. (2020). Transition Metal Dichalcogenide–Silk Nanofibril Membrane for One-Step Water Purification and Precious Metal Recovery. *ACS Applied Materials & Interfaces*, *12*(21), 24521–24530. https://doi.org/10.1021/ACSAMI.0C07846

Zhao, R., Satpradit, O., Rijnaarts, H. H. M., Biesheuvel, P. M., & van der Wal, A. (2013). Optimization of salt adsorption rate in membrane capacitive deionization. *Water Research*, *47*(5), 1941–1952. https://doi.org/10.1016/J.WATRES.2013.01.025

APPENDICES

APPENDIX A

CALIBRATION CURVES

Figure A1 Calibration Curve For A) Copper Nitrate B) Nickel Nitrate, And C) Chromium Nitrate Aqueous Solution

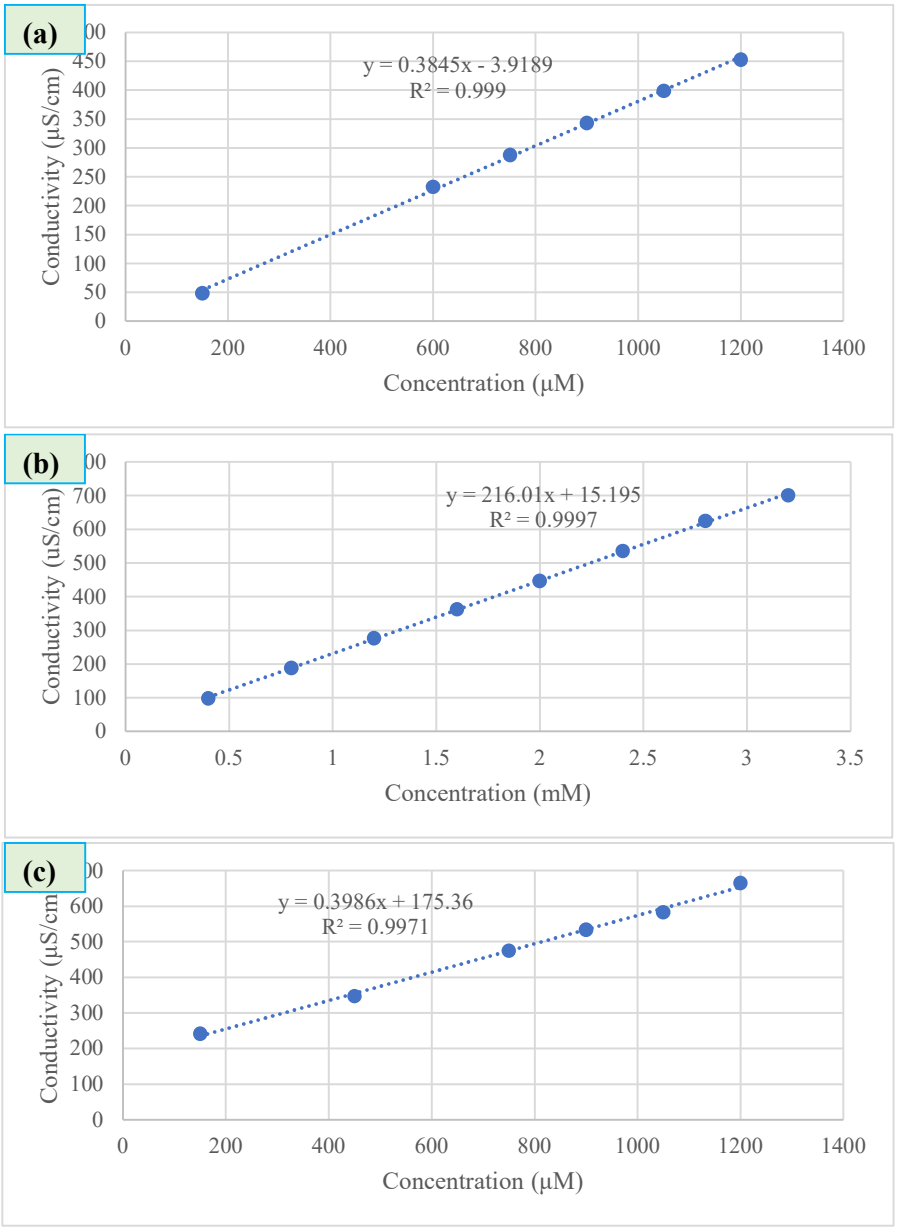

Figure A2 Calibration Curve For A) Copper Nitrate And B) Chromium Nitrate Aqueous Solution Using AAS.

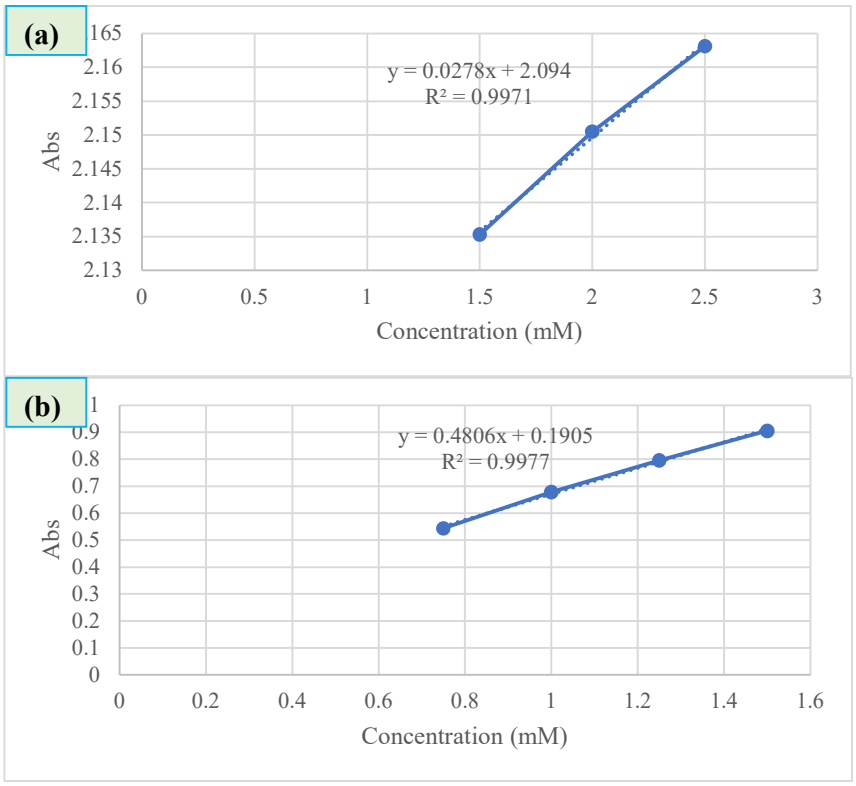

APPENDIX B

EXAMPLE CURRENT PROFILE DURING METAL RECOVERY

Figure A1 Current vs Time Profile Using a) 0.5mM and b) 1.5mM Copper Solution.

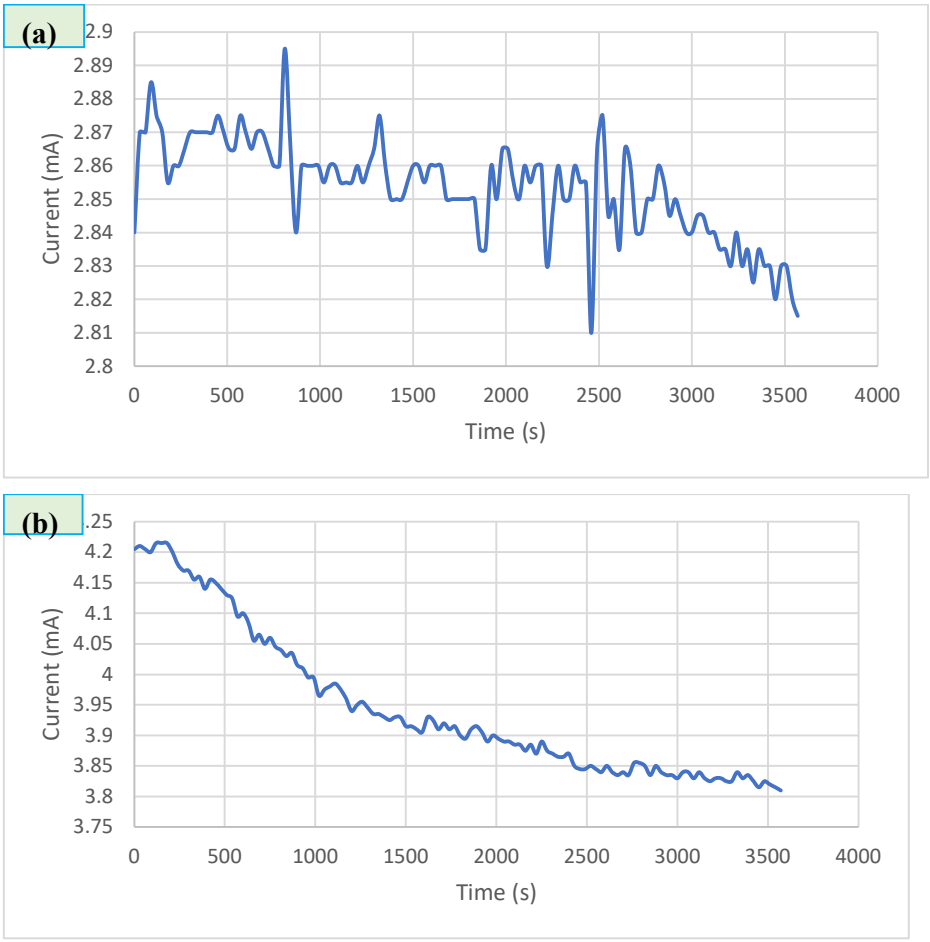

Figure A2 Current vs Time Profile Using a) 0.5mM and b) 1.5mM Nickel Solution.

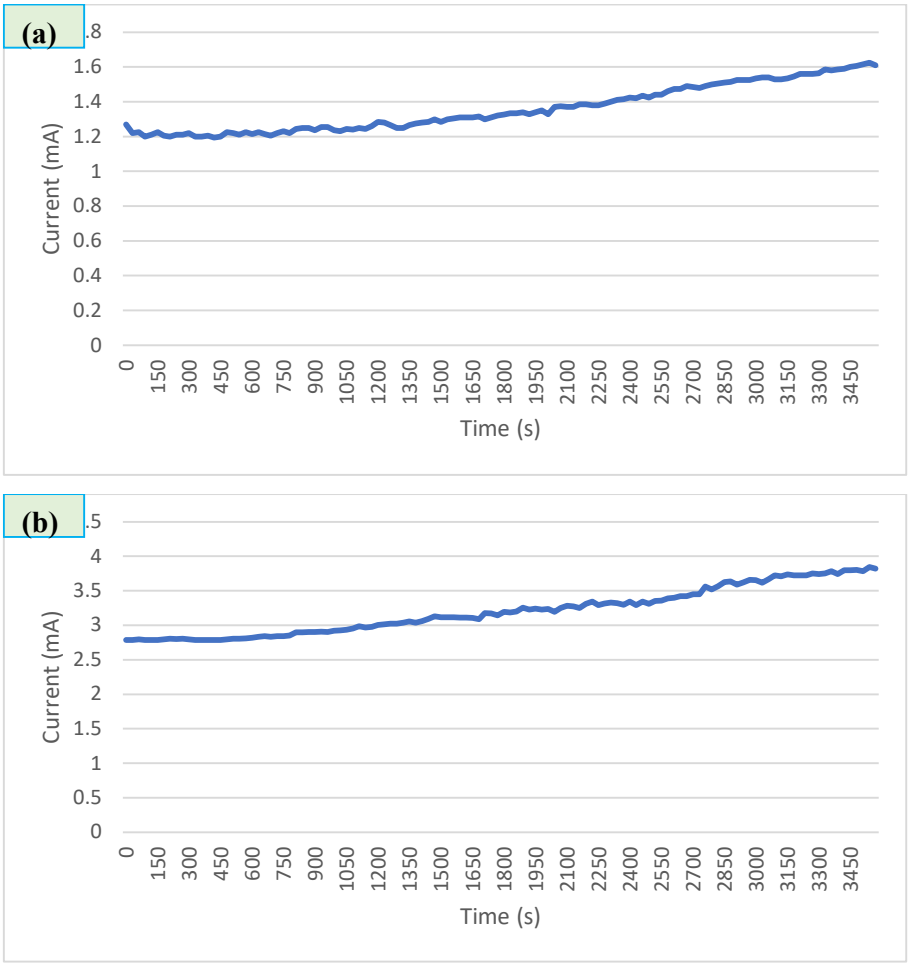

Figure A3 Current vs Time Profile Using a) 0.5mM and b) 1.5mM Chromium Solution.

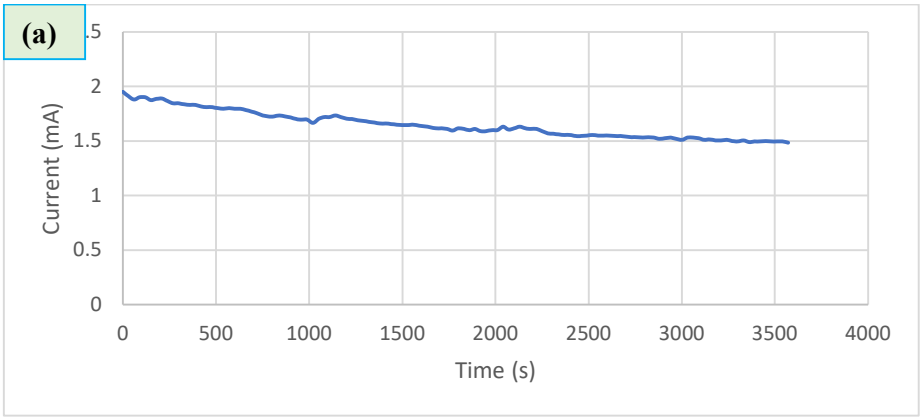

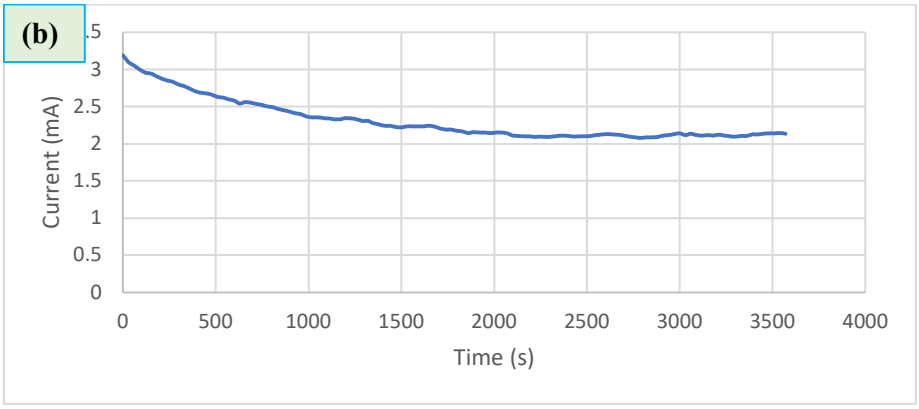
(b)
Current (mA)
3.5
3
2.5
2
1.5
1
0.5
0
0
500
1000
1500
2000
2500
3000
3500
4000
Time (s)

APPENDIX C

CURRENT PROFILE USING PLAIN ACC BASED CDI CELL

Figure A1 Charging Current over Time Graph of the CDI Cell for Adsorption Cycle; a) 2000 ppm and b) 3000 ppm

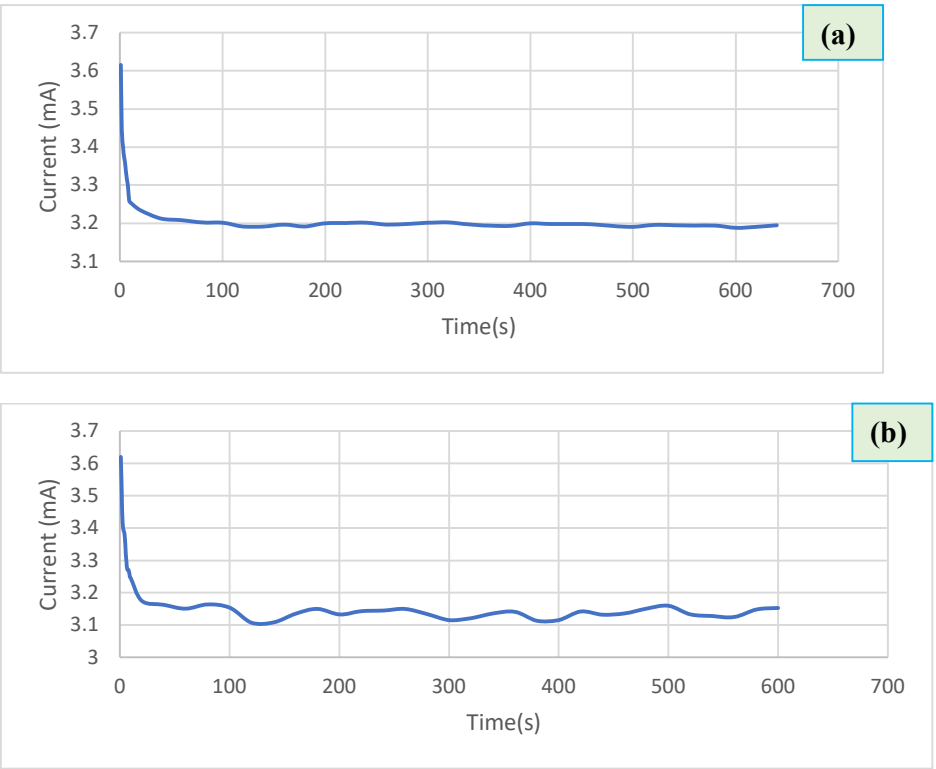

The current exhibit the characteristic of CDI adsorption. The current gradually reduced after the step input of the voltage across the CDI until it slowed and reached a plateau, similar to the following graph. Based on the result, it can also be presumed that the adsorption of NaCl using plain ACC happens within 100 seconds. There does not seem to be any significant effect of NaCl concentration on the characteristic of the current.

Figure A2 Current Over Time Graph of The CDI Module For Desorption Cycle Using 2000 Ppm NaCl Solution

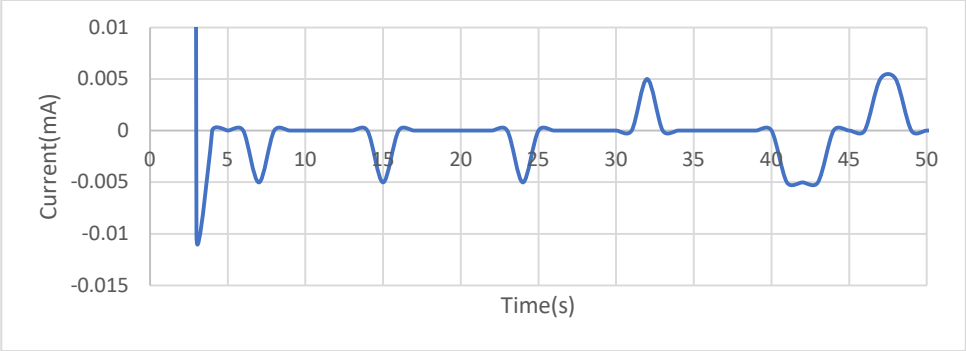

According to Figure A2, the current graph during desorption is expected to show sudden flow of current in the opposite direction. However, the voltage difference is too small, and the desorption process is too fast for data collection, causing the plotted graph to be too unreliable to be used. However, it is presumed from the graph that the sudden spike in the graph of desorption happened within 10 seconds, as shown from the plotted graph.

To resolve the issues mentioned above, the adjustment was made to investigate the error resulting from the current reaching a plateau at 3 mA instead of zero. It was found that by adjusting the size of the filter paper to a bigger size (length) than the carbon cloth, the current no longer exhibits the base value of 3 mA previously observed. We speculated that this was due to the small contact point between both electrodes.

APPENDIX D

COPPER RECOVERY EXTRA DATA

Figure A1 Stainless Steel After Copper Deposition At 1.5V And 2.0V And 30 Minutes Duration

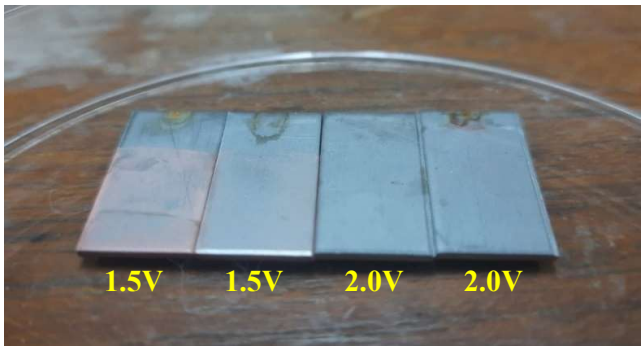

Table A1 Mass Measurement After and Before Copper Deposition.

Applied Voltage	Theoretical deposit mass (mg)/3.50 cm^2	Actual deposit mass(mg)/3.50 cm^2
1.5V	0.39	0.93
	0.39	0.30
2.0V	4.58	0.20
	5.65	0.47

This set of metal recovery was the very first batch of depositions. The theoretical deposit mass and actual deposit mass were way different because we mistakenly changed the weight machine before and after the deposition. Moreover, we measured the initial weight before washing with the acetone. This set of metal recovery was the very first setup; therefore, some unexpected issues occurred.

Figure A2 Stainless Steel After Copper Deposition At 2.0V And 3.0 V

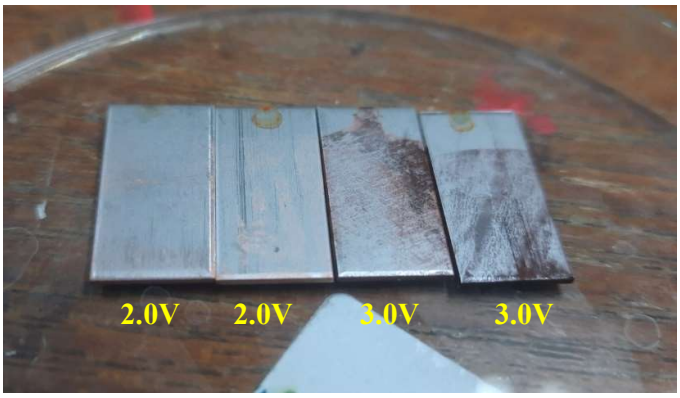

Table 2 Mass Measurement After and Before Copper Deposition To The Stainless Steel At pH of 1.9.

Applied Voltage	**Theoretical deposit mass (mg)/3.50 cm^2**	**Actual deposit mass(mg)/3.50 cm^2**
2.0V	1.61	1.71
	1.63	1.65
3.0V	4.40	3.35
	5.65	3.65

APPENDIX E

EFFECT OF APPLIED VOLTAGE ON DIFFERENT METAL

Table A1 Effects of applied voltage on different metal species recovery

	Actual deposit mass (mg)/3.50 cm^2		
Applied Voltage (V)	Copper	Nickel	Chromium
1.5	0.93	-	-
1.7	1.91	-	-
2.0	3.55	-	0
2.5	4.55	-	-
3.0	5.72	-	0.03
4.0	-	-	0.04
5.0	-	5.69	0. 46
5.5	-	4.48	-
6.0	-	-	0. 48
7.0	-	-	0. 26

APPENDIX F

EFFECT OF DIFFERENT CONCENTRATION ON METAL

Table A1 Comparison of mass change using different concentration on different metal ion.

	Actual deposit mass (mg)/3.50 cm^2		
Concentration	Copper	Nickel	Chromium
0.5 mM	0.01	0.648	0.935
1.5 mM	0.03	1.646	1.8725
1.6 mM	0.05	1.938	1.8925
3.0 mM	0.06	2.82	2.0575

APPENDIX G
CHARACTERIZATION USING AAS

Table A1 Copper Recovery and Efficiency Data by Varying Concentration

Concentration	pH	Actual deposit mass (mg)/3.41cm^2	Copper Recovery Efficiency
0.5mM	1.97	1.96	42%
		2.19	52%
1.5mM		2.75	46.6%
		2.96	44.6%

Table A2 Chromium Recovery and Efficiency Data By Varying Concentration

Concentration	Theoretical Deposit mass (mg)/3.41cm^2	Actual deposit mass (mg)/3.41cm^2	Chromium Recovery Efficiency
0.5mM	0.96	1.02	34.72%
	1.07	1.03	37.88%
1.5mM	2.00	1.86	19.53%
	1.75	2.53	17.26%

APPENDIX H

EXAMPLE CDI CHARGING AND DISCHARGING CURRENT

Figure 1 CDI Discharging Current and SC Charging Current Vs. Time Profile Using A) Copper, B) Nickel, And C) Chromium Ion Solution.

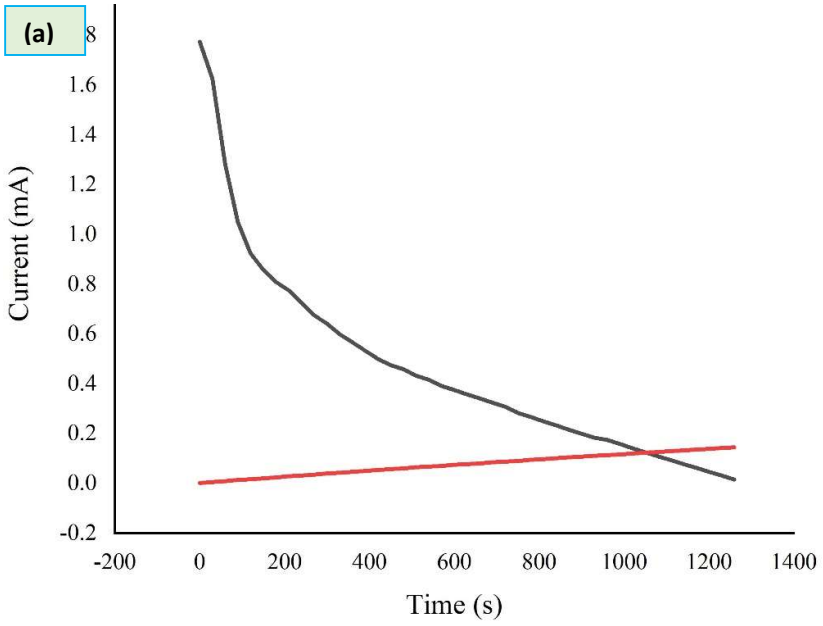

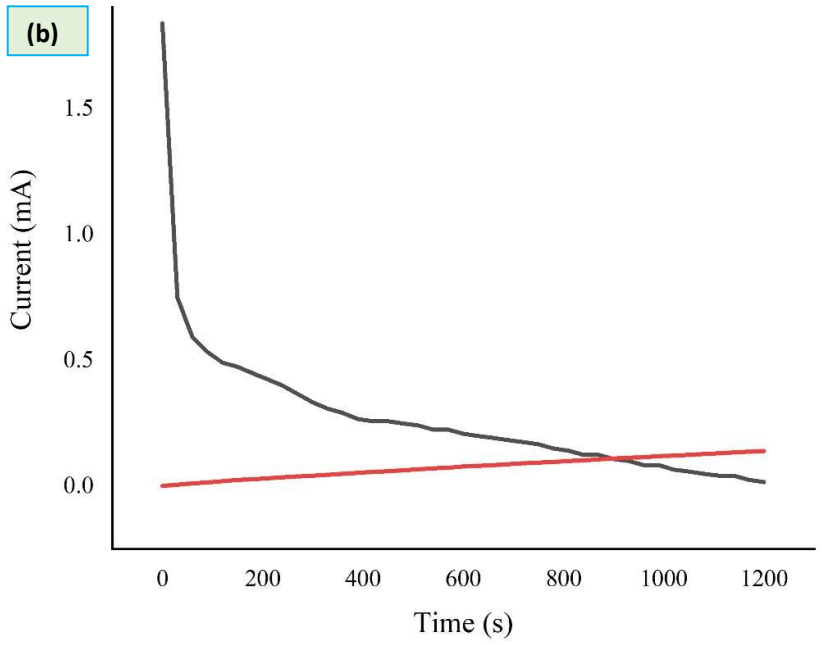

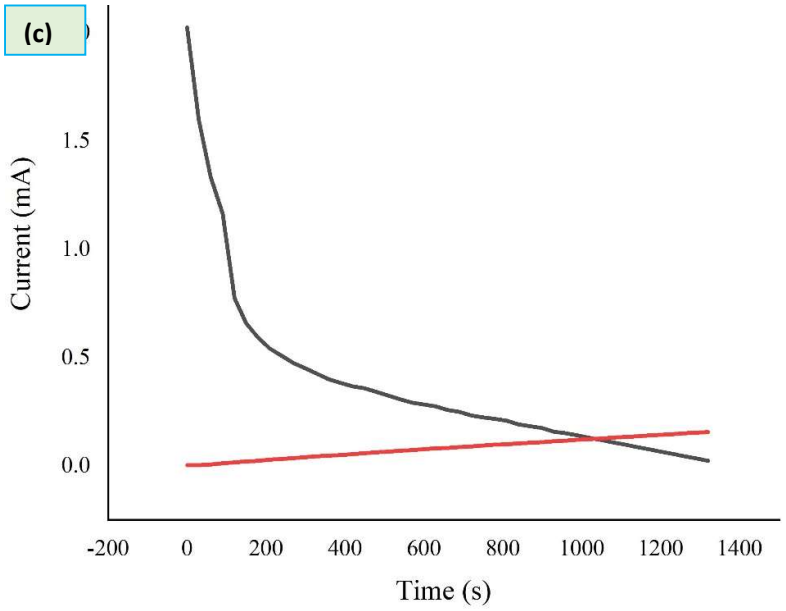
(c)
1.5
1.0
0.5
0.0
Current (mA)
-200
0
200
400
600
800
1000
1200
1400
Time (s)